Electronic Supplementary Material (ESI) for Chemical Science.

Supporting Information for

Exploring Cu/Al cluster growth and reactivity: From embryonic building blocks to intermetalloid, open-shell superatoms.

Max Schütz[a] [b], Christian Gemel[a] [b], Maximilian Muhr[a] [b], Christian Jandl [b], Samia Kahlal [c], Jean-Yves Saillard[c] and Roland A. Fischer*[a] [b]

[a] Department of Chemistry, Technical University Munich, Lichtenbergstrasse 4, D-85748 Garching, Germany

[b] Catalysis Research Centre, Technical University Munich, Ernst-Otto-Fischer Strasse 1,D-85748 Garching, Germany

[c] Univ Rennes, CNRS, ISCR-UMR 6226, F-35000 Rennes, France

* corresponding author

Content

1. Materials and Methods

Spectroscopy NMR spectra were recorded on a Bruker Avance III AV400US (1H, 400 MHz). The deuterated solvents were degassed and stored over molecular sieves. Chemical shifts are given relative to TMS and were referenced to the residual solvent peak as internal standards. Chemical shifts are reported in parts per million, downfield shifted from TMS, and are consecutively reported as position (δH or δC), relative integral, multiplicity (s = singlet, d = doublet, q = quartet and m = multiplet) and assignment. Variable temperature (VT) NMR spectra were recorded on a Bruker DRX 400 spectrometer (^{1}H, 400 MHz). FT-IR spectra were measured in an ATR setup with a Bruker Alpha FTIR spectrometer under an inert gas atmosphere in a glove-box.

Elemental Analysis (EA) EA measurements were conducted in the Microanalytical Laboratory Kolbe in Mülheim an der Ruhr.

Spectrometry Mass spectrometry was conducted on filtered solutions with an Exactive™ PlusOrbitrap system from the Thermo Scientific company and a Micromass LCT-QTOF-Micro mass spectrometer; Ionisation method: Liquid injection field desorption ionization (LIFDI; special ionization cell obtained from Linden CMS GmbH, Leeste, Germany; http://www.linden-cms.de), solvent: toluene. The sample is applied on a tungsten wire which is coated with thousands of micro graphite dendrites. By applying a potential between the emitter and the counter electrode of 10 kv the sample molecules are ionised and subsequently accelerated to the counter electrode and eventually to the detector. The resulting ions are radical cations, e.g. [M]•+. Accordingly, all LIFDI-MS spectra presented in this work are recorded in the positive ion mode.

For GC-MS measurements few drops of water were added to the respective diluted reaction solution in toluene. The mixture was filtered over neutral aluminium oxide and afterwards again over standard filter paper. Measurements were conducted on a Agilent GC-7890 with Autosampler.

TEM measurements

Samples were measured by High Resolution Transmission Electron Microscope (HRTEM) Titan G2 (FEI) with Image corrector on accelerating voltage 80 kV. STEM images were taken with HAADF detector 3000 (Fishione). Energy Dispersive Spectrometry (EDS) was performed by Super-X system with four silicon drift detectors (Bruker).

1. Materials and Methods

X-ray crystallography

Data were collected on a single crystal x-ray diffractometer equipped with a CMOS detector (Bruker APEX III, κ-CMOS), a TXS rotating anode or an IMS microsource (see Table S4) with MoK_α radiation (λ = 0.71073 Å) and a Helios optic using the APEX3 software package.[C1] Measurements were performed on single crystals coated with perfluorinated ether. The crystals were fixed on top of a kapton micro sampler and frozen under a stream of cold nitrogen. A matrix scan was used to determine the initial lattice parameters. Reflections were corrected for Lorentz and polarisation effects, scan speed, and background using SAINT.[C2] Absorption correction, including odd and even ordered spherical harmonics was performed using SADABS.[C3] Space group assignments were based upon systematic absences, E statistics, and successful refinement of the structures. The structures were solved using SHELXT with the aid of successive difference Fourier maps, and were refined against all data using SHELXL-2014/2017 in conjunction with SHELXLE.[C4,C5,C6] Hydrogen atoms were calculated in ideal positions as follows: Methyl hydrogen atoms were refined as part of rigid rotating groups, with a C–H distance of 0.98 Å and $U_{iso(H)} = 1.5 \cdot U_{eq(C)}$. Other H atoms were placed in calculated positions and refined using a riding model, with methylene and aromatic C–H distances of 0.99 Å and 0.95 Å, respectively, other C–H distances of 1.00 Å, all with $U_{iso(H)} = 1.2 \cdot U_{eq(C)}$. Non-hydrogen atoms were refined with anisotropic displacement parameters. Full-matrix least-squares refinements were carried out by minimizing $\Sigma w(F_o^2 - F_c^2)^2$ with the SHELXL weighting scheme.[C5] Neutral atom scattering factors for all atoms and anomalous dispersion corrections for the non-hydrogen atoms were taken from *International Tables for Crystallography*.[C7] A split layer refinement was used for disordered groups and additional restraints on distances, angles and anisotropic displacement parameters were employed to ensure convergence within chemically reasonable limits, if necessary. Heavily disordered solvent molecules were treated as a diffuse contribution to the overall scattering without specific atom positions using the PLATON/SQUEEZE procedure.[C8] Images of the crystal structures were generated with Mercury and PovRay (illustration of polyhedra).[C9, C10]

Computational Details

Density Functional Theory (DFT) calculations[C11] were carried out with the use of the Amsterdam Density Functional code (ADF2017).[C12] with the addition of Grimme's D3 empirical corrections[C13] in order to take into account dispersion effects. The triple-ξ Slater basis set plus two polarization functions (STO-TZP),[C14] was used, together with the Becke-Perdew (BP86)[C15, C16] exchange-correlation functional. All the optimized structures were confirmed as true minima on their potential energy surface by analytical vibration frequency calculations. Natural atomic orbital (NAO) populations and Wiberg bond indices were computed with the natural bond orbital NBO6.0 program[C17] implemented in the ADF2017 package. The NMR chemical shifts were computed according to the gauge-independent atomic orbitals (GIAO) method,[C18] assuming the Zero Order Regular Approximation (ZORA) for the S = ½ complex **3_H**.[C19]

2. Synthesis

General

All experiments were conducted using standard Schlenk and glovebox techniques under an atmosphere of purified argon. All solvents were carefully dried (water content < 5 ppm) and saturated with argon prior to their use. The starting compounds AlCp*, CuMes = $[Cu_5](Mes)_5$ and $(TMS)_3SiBr$ were prepared according to literature methods.[1, 2]

Synthesis of $[Cu_4Al_4](Cp*)_5(Mes)$ (1)

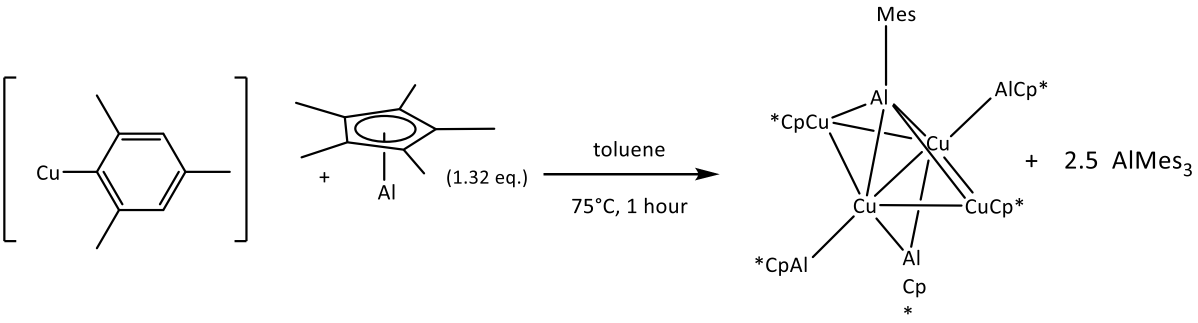

1

Scheme S1: Synthesis of $[Cu_4Al_4](Cp*)_5(Mes)$ (**1**).

232.56 mg (1.4 mmol, 1.31 eq.) of AlCp* and 200 mg (1.1 mmol, 1 eq.) of CuMes were dissolved in 20 ml of toluene and heated to 75 °C for 60 minutes resulting in a dark green solution. The solution was filtered *via* canula, concentrated under reduced pressure (10 ml) and left for crystallization at -30 °C for one week. The resulting needle-like crystals were isolated, washed with *n*-hexane (3 x 0.25 ml) and recrystallized from a minimum amount of toluene at -30 °C giving pure **1** in 5 % yield (based on Cu).

^{1}H-NMR (400mHz, 298 K, toluene-d_8): 6.90 (s, 2H, CH_{aryl}(Mes)), 2.31 (s, 3H, -CH_3(Mes)), 2.28 (s, 6 H, -CH_3(Mes)), 2.10 (s, 30H, -CH_3(CuCp*)), 1.97 (s, 15H, -CH_3(AlCp*$_{bridging}$)), 1.92 (s, 30H, -CH_3(AlCp*$_{apical}$)). ^{13}C-NMR (400 mHz, 298 K, toluene-d_8): 143.10 (s, quaternary C(Mes)), 126.79 (s, quaternary C(Mes)), 115.37 (s, quaternary C(AlCp*)), 114.45 (s, quaternary C(AlCp*)), 103.39 (s, quaternary C(CuCp*)), 32.46 (s, CH$_3$(Mes)), 25.23 (s, -CH$_3$(Mes)), 13.13 (s, -CH$_3$(CuCp*)), 11.97 (s, -CH$_3$(AlCp*)), 10.78 (s, -CH$_3$(AlCp*)).

IR (ATR, 298 K): ν [cm^{-1}] = 2897 (b), 2835 (b), 1482 (w), 1415 (s), 1376 (s), 1376 (s), 1023 (w), 846, 800, 731 (w), 590, 538 (w), 453 (s, i), 422 (s).

Elemental analysis [%]: Calculated for $Cu_4Al_4C_{59}H_{86}$: C: 61.22, H: 7.49, Al: 9.32, Cu: 21.96; found: C: 60.14, H: 7.61, Al: 9.25, Cu: 21.68.

*Note: Despite the reaction being rather selective according to in-situ NMR analysis, pure **1** is only accessible in small yields (5 %) due to very similar solubility properties of **1** and side products (AlCp*Mes$_2$, AlMes$_3$) requiring profound washing and recrystallization procedure.*

Synthesis of $[CuAl_2](Cp^*)_3$ (2)

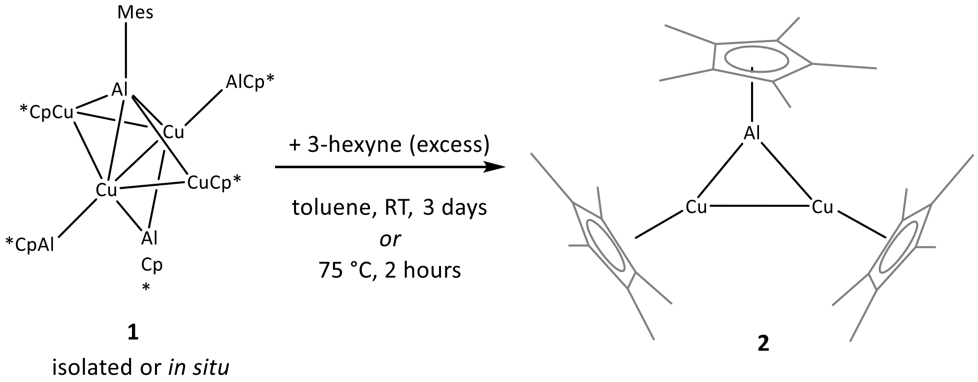

Scheme S2: Synthesis of $[Cu_2Al](Cp^*)_3$ (**2**).

232.6 mg (1.4 mmol, 1.31 eq.) of AlCp* and 200 mg (1.1 mmol, 1 eq.) of CuMes were dissolved in 20 ml of toluene and heated to 75 °C for 60 minutes resulting in a dark green solution. 3 ml (26.4 mmol, 24 eq.) of 3-hexyne were added under vigourous stirring resulting in a color change to dark brown. The solution was heated to 75 °C for 60 minutes, filtered via canula, concentrated under reduced pressure (10 ml) and left for crystallization at -30 °C for one week. The resulting yellow-orange crystals were isolated, washed with *n*-hexane (3 x 0.3 ml) and dried to yield pure **2** in 14 % yield (based on Cu).

^{1}H-NMR (400mHz, 298 K, benzene-d$_6$): 2.32 (s, 30H, -CH_3(CuCp*)), 1.70 (s, 15H, -CH_3(AlCp*)). ^{13}C-NMR (400 mHz, 298 K, benzene-d$_6$): 115.82 (s, quaternary C(AlCp*)), 104.32 (s, quaternary C(CuCp*)), 12.55 (s, -CH$_3$(CuCp*)), 9.87 (s, -CH$_3$(AlCp*).

IR (ATR, 298 K): ν [cm^{-1}] = 2894 (b), 2848 (b), 2716 (w), 1480 (w), 1425, 1375, 1261 (w), 1160 (w), 1049-1115 (w), 1020, 799, 729, 694, 591, 518 (i), 430, 420.

Elemental analysis [%]: Calculated for $Cu_2AlC_{30}H_{45}$: C: 64.37, H: 8.10, Al: 4.82, Cu: 22.70; found: C: 63.22, H: 8.01, Al: 4.89, Cu: 22.02.

2. Synthesis

Synthesis of $[Cu_{7/8}Al_6](Cp^*)_6$ (3/4)

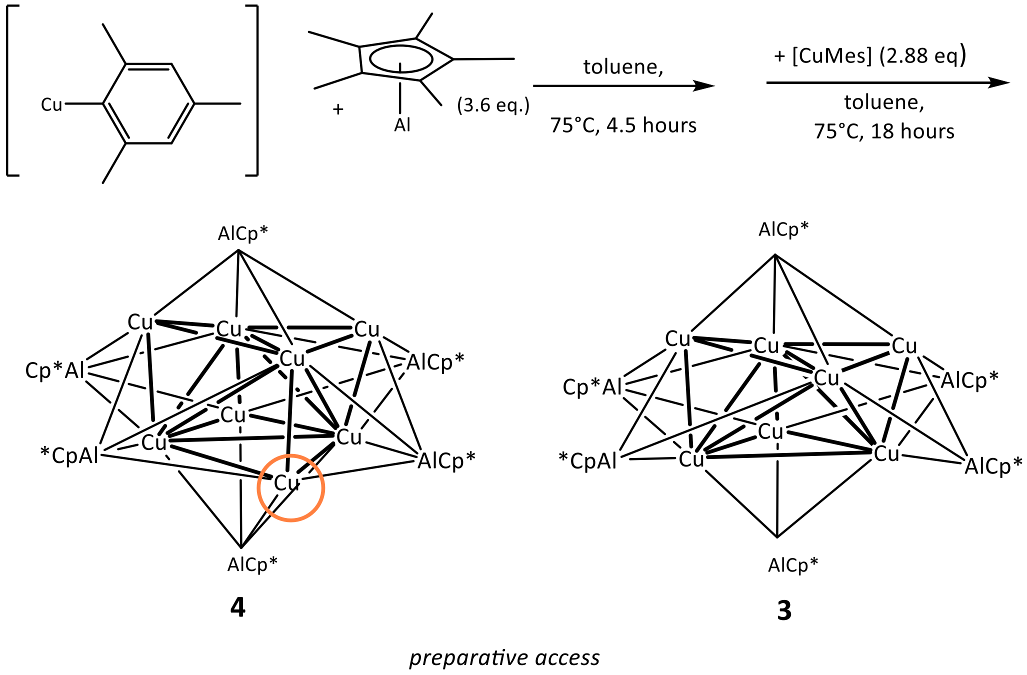

Scheme S3: Synthesis of $[Cu_{7/8}Al_6](Cp^*)_6$ (**3/4**).

500 mg (3.1 mmol, 1 eq.) of AlCp* and 156.3 mg (0.86 mmol, 0.28 eq.) of CuMes were suspended in 50 ml of toluene and heated to 75 °C for 4.5 hours resulting in a deep-green solution. Additional 305 mg (1.7 mmol, 0.55 eq.) CuMes were added and the mixture was heated to 75 °C for 24 hours. The dark-brown solution was concentrated under reduced pressure to half its volume and cooled to -30 °C for 7 days. The black precipitate was isolated by means of canula filtration, washed with hexane at -78 °C (4 x 0.4 ml) and dried under reduced pressure to yield **3/4** in 23 % yield.

^{1}H-NMR (400mHz, 298 K, 0.007 mmol/ml, benzene-d_6): 1.94 ppm (s, $[Cu_8Al_6](Cp^*)_6$), -1.03 ppm (broad paramagnetic signal, $[Cu_7Al_6](Cp^*)_6$), ^{13}C-NMR (400 mHz, 298 K, benzene-d_6): 115.19 (s, quaternary C($[Cu_8Al_6](Cp^*)_6$)), 12.89 (s, -CH_3(($[Cu_8Al_6](Cp^*)_6$)).

IR (ATR, 298 K): 2962 (w), 2903, 2850, 1489 (w), 1423 (s), 1369 (s), 1264 (w), 1157-1017 (b), 799, 729, 587 (w), 414 (s, i);

Elemental analysis [%]: Calculated for $Cu_8Al_6C_{60}H_{90}$: C: 48.64, H: 6.12, Cu: 34.31, Al: 10.93; found: C: 48.16, H: 6.04, Cu: 34.77, Al: 10.76.

*Note: The synthesis of **3/4** turned out to be very sensitive even to subtle changes of reaction conditions. Small variations of the CuMes:AlCp* ratio employed resulted in isolation of a mixture of **3/3$_H$/4** instead of **3/4**. In situ ^{1}H-NMR analysis suggests Cp* to be the origin of the hydride ligand in these cases, as pentamethylfulvene was detected as a reaction product. The stepwise addition of CuMes allowed for a better reaction control and isolation of pure **3/4** as described above.*

Synthesis of [H_3Cu_3](dppbz)$_3$ (dppbz = 1.2-bis(diphenylphosphinobenzene)

68.1 mg (0.035 mmol, 1 eq.) of [H_6Cu_6](PPh_3)$_6$ and 95.3 mg (0.21 mmol, 6 eq.) of dppbz were suspended in 1.5 ml of toluene and stirred for several hours resulting in a color change from red to yellow. The solution was kept standing without stirring overnight resulting in a yellow precipitate, which was subsequently isolated by filtration. After recrystallized from 0.5 ml of hot toluene, [H_3Cu_3](dppbz)$_3$ was isolated as yellow powder in 50 % yield based on Cu. ^{1}H- and ^{31}P-NMR analysis of the product is consistent with values reported in literature.[3]

Synthesis of (TMS)$_3$SiD

2.5 g (7.6 mmol, 1 eq.) of (TMS)$_3$SiBr and 300 mg (1.04 eq.) of $LiAlD_4$ were heated in 100 ml diethylether under reflux conditions for three days under argon atmosphere. 1M KOH solution (50 ml) in water was added slowly and the mixture was extracted three times with diethylether. The organic layer was separated, dried over anhydrous $MgSO_4$, filtered and the solvent was removed under reduced pressure resulting in (TMS)$_3$SiD in 50 % yield, which was dried over molecular sieve for further use.

^{1}H-NMR (toluene-d$_8$): 0.24 (s, 27H, Si-*CH_3*).

2. Synthesis

Table S1: Access to different Cu/Al cluster composites as determined by LIFDI-MS analysis.

conditions	reaction	product composite obtained	crystal structure	preparative synthesis possible
A	$[Cu(dppbz)H]_3$ + AlCp*	$\mathbf{3_H/4}$	yes	no
B	CuMes + AlCp*	**3/4**	no	yes
C	thermal treatment **1**	$\mathbf{3/3_H/4}$	no	no
D	**3/4** + CuMes	**4**	yes*	no
E	**2** + CuMes	**4**	yes	no
F	thermal treatment **3/4** (toluene)	$\mathbf{3/3_H/4}$	no	no
G	**3/4** + $(TMS)_3SiH$	$\mathbf{3/3_H/4}$	no	no
H	**3/4** + $(TMS)_3SiD$	$\mathbf{3/3_H/3_D/4}$	no	no

dppbz = 1,2-bis(diphenylphosphino)benzene

Likewise to entry F, a crystal structure of* ***4* *was obtained for conditions H, showing a* $[Cu_8]$ *kernel with fully occupied Cu positions.*

Experimental procedures for conditions described in Table S1

Conditions A: Reaction of $[H_3Cu_3](dppbz)_3$ with AlCp* / Synthesis of $3_H/4$

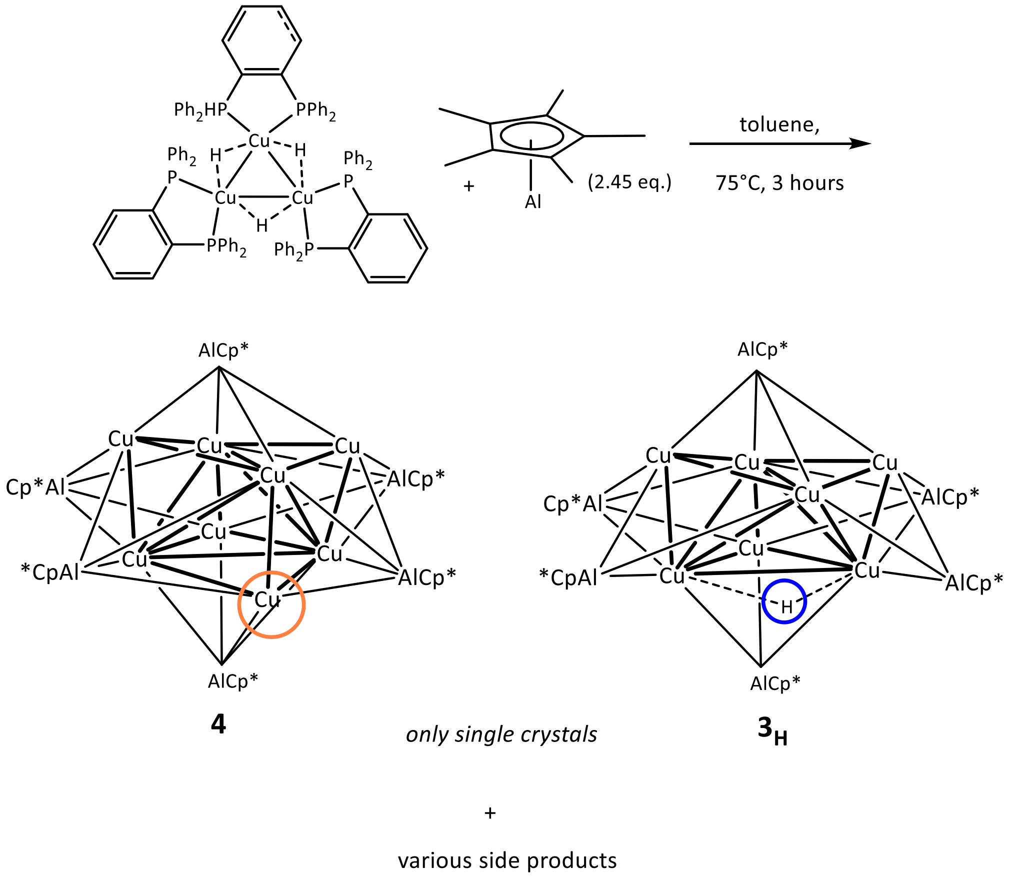

Scheme S4: Synthesis of $[Cu_{7/8}Al_6](Cp^*)_6$ (**3_H/4**).

20 mg (13.0 µmol, 0.4 eq.) $[H_3Cu_3](dppbz)_3$ and 5.20 mg (0.032 mmol, 1.0 eq.) AlCp* were heated at 75 °C for 2 h in 2.5 mL toluene resulting in a dark solution. Cooling the concentrated and filtered reaction solution to -30 °C for several days leads to an inseperable mixture of few dark single-crystals of **3_H/4** suitable for SC-XRD in addition to free dppbz ligand and other side-products.

For *in-situ* LIFDI-MS experiments, the synthesis of **3_H/4** can also be conducted as follows:

12.3 mg (6.27 µmol, 0.2 eq.) of $[H_6Cu_6](PPh_3)_6$, 5 mg (0.031 mmol, 1 eq.) of AlCp* and 3.4 mg (7.62 µmol, 1.2 eq) of dppbz were heated in 1 ml of toluene for three hours resulting in a dark solution. In the same manner, preparation of **3_D/4** was conducted using $[D_6Cu_6](PPh_3)_6$ as starting material.

Conditions C: Thermal treatment of 1

5 mg (4.3 µmol) of isolated **1** were dissolved in 0.5 ml of toluene-d_8 or benzene-d_6 in a sealed Young-NMR tube and heated to 75 °C for six hours.

Conditions D: Conversion of isolated 3/4 with CuMes

5 mg (3.4 µmol, 1 eq.) of isolated **3/4** and 3.1 mg (0.017 mmol, 5 eq.) of CuMes were dissolved in 0.5 ml of benzene-d6 in a sealed Young-NMR tube and heated to 75 °C for several hours.

10 mg (6.8 µmol, 1 eq.) of isolated **3/4** and 12.4 mg (0.068 mmol, 10 eq.) of CuMes were dissolved in 1 ml of toluene and heated to 75 °C for 5 hours resulting in a metallic precipitate (Cu). Filtration of the solution and storage at -30 °C led to crystallization of pure **4** as determined by SC-XRD in very small yield.

Conditions E: Conversion of 2 with CuMes

5 mg (8.9 µmol, 1 eq.) of isolated **2** and 1.9 mg (10.4 µmol, 0.4 eq) of CuMes were dissolved in 0.5 ml of benzene-d_6 in a sealed Young-NMR tube and heated to 75 °C for 6 hours. Conducting the reaction toluene and cooling the filtered reaction solution to -30 °C for several weeks led to few single crystals of pure **4** as determined by SC-XRD.

Conditions F: Thermal treatment of 3/4

5 mg (3.4 µmol) of isolated **3/4** were heated in 0.5 ml of toluene to 110 °C for 5 days in a sealed Young-NMR tube.

Conditions G/H: Conversion of isolated 3/4 with excess $(TMS)_3SiH$ and $(TMS)_3SiD$

10 mg (6.8 µmol) of isolated **3/4** and 0.3 ml (1 mmol) of $(TMS)_3SiH$ / 0.3 ml (1 mmol) of $(TMS)_3SiD$ were dissolved in 2.5 ml of toluene and heated to 110 °C for 5 days.

For the *in-situ* ^1H NMR reaction, 5 mg (3.4 µmol) of isolated **3/4** and 10 mg (40.3 µmol) of $(TMS)_3SiH$ were dissolved in 0.5 ml of toluene-d_8 and heated to 110 °C for 5 days.

3. NMR analysis

3.1 Time dependant analysis

Figure S1: *In-situ* ^{1}H-NMR spectra (benzene-d$_6$) of the reaction CuMes + AlCp* (1:1.3), 75 °C.

3. NMR analysis

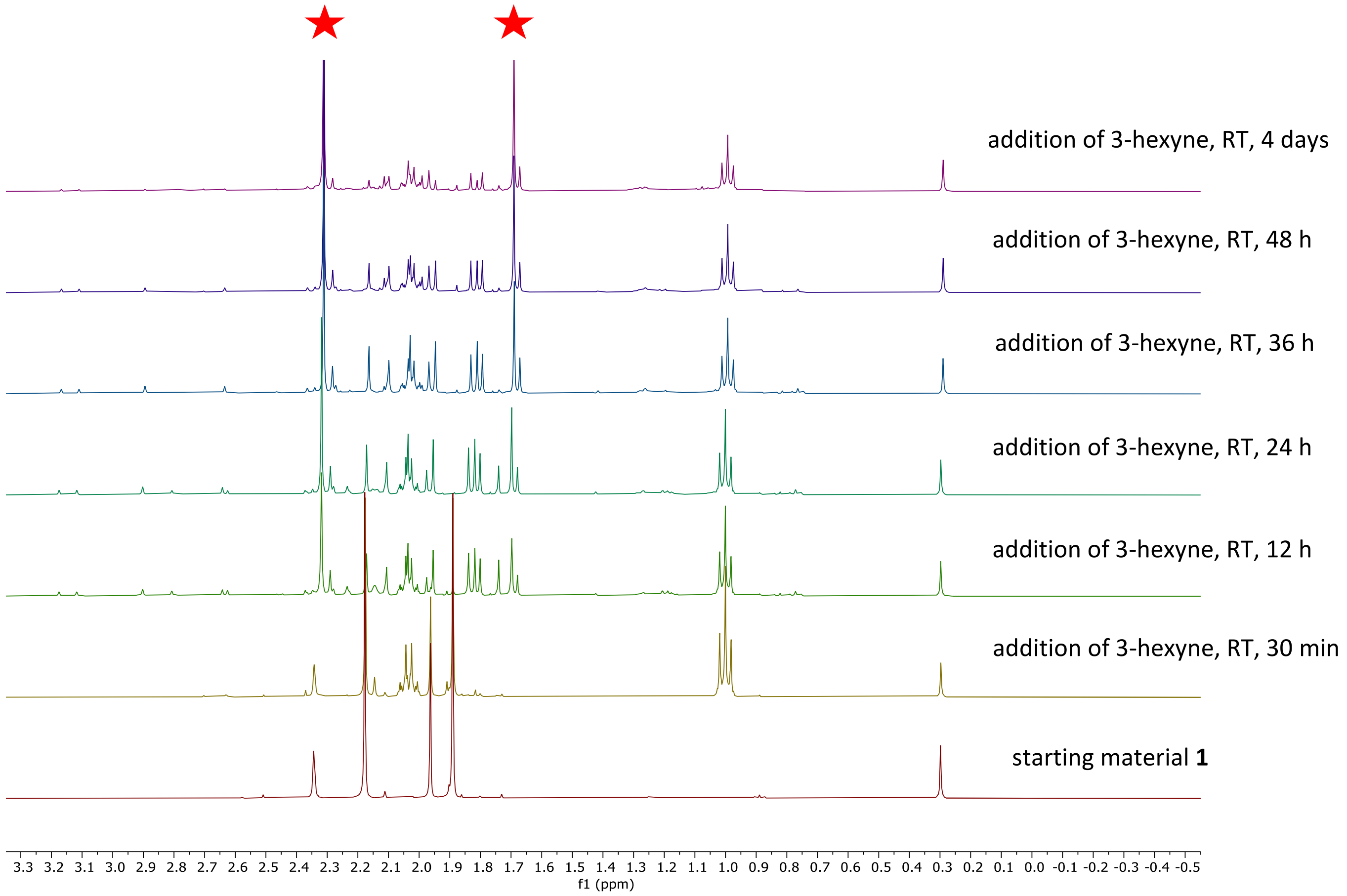

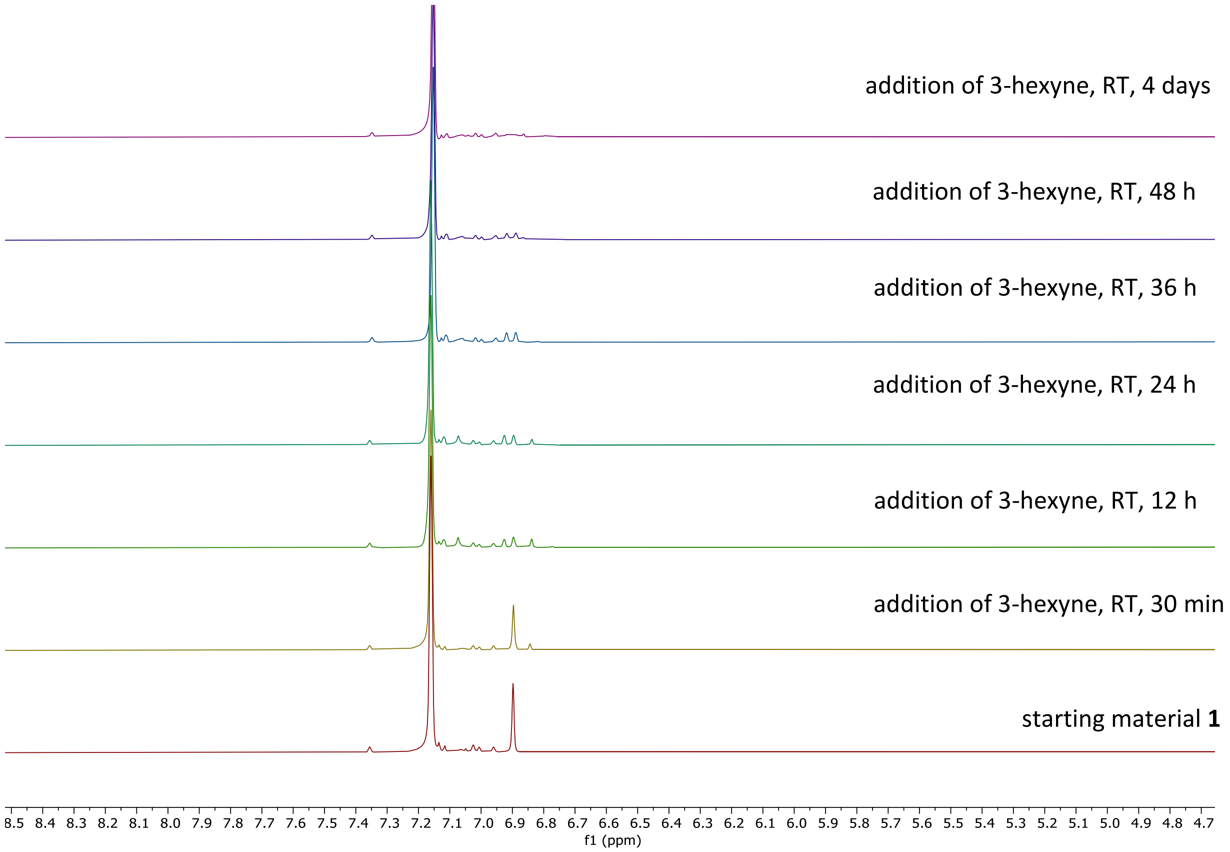

★ = $[Cu_2Al](Cp^*)_3$

Figure S2: *In-situ* ^{1}H NMR spectra (benzene-d$_6$) of the conversion of **1** with 3-hexyne (8 eq.). Up: Aliphatic region, Bottom: Aromatic region of the spectra.

3. NMR analysis

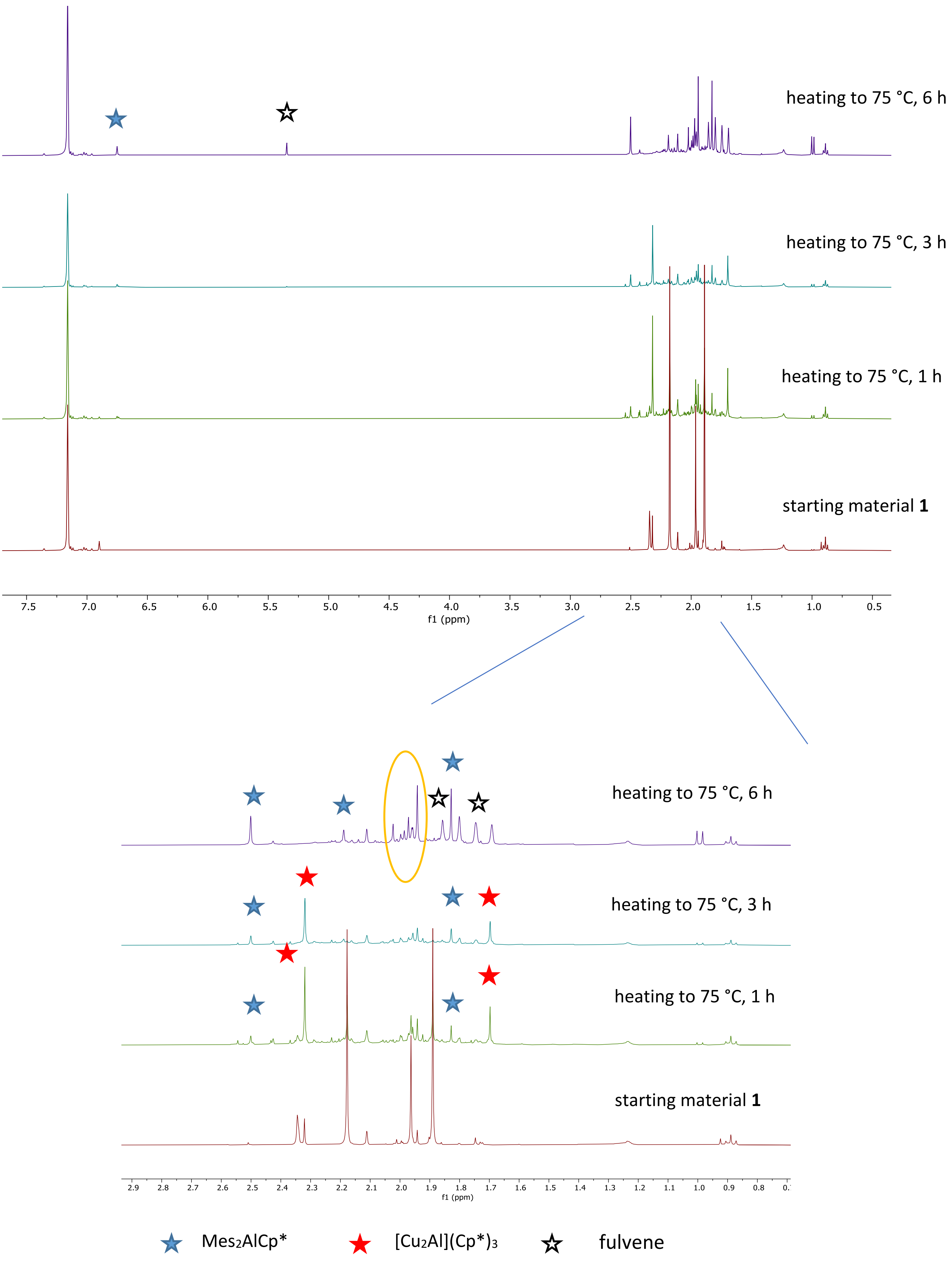

Figure S3: *In situ* ^{1}H-NMR spectra (benzene-d$_6$) of heating isolated compound **1**.

3. NMR analysis

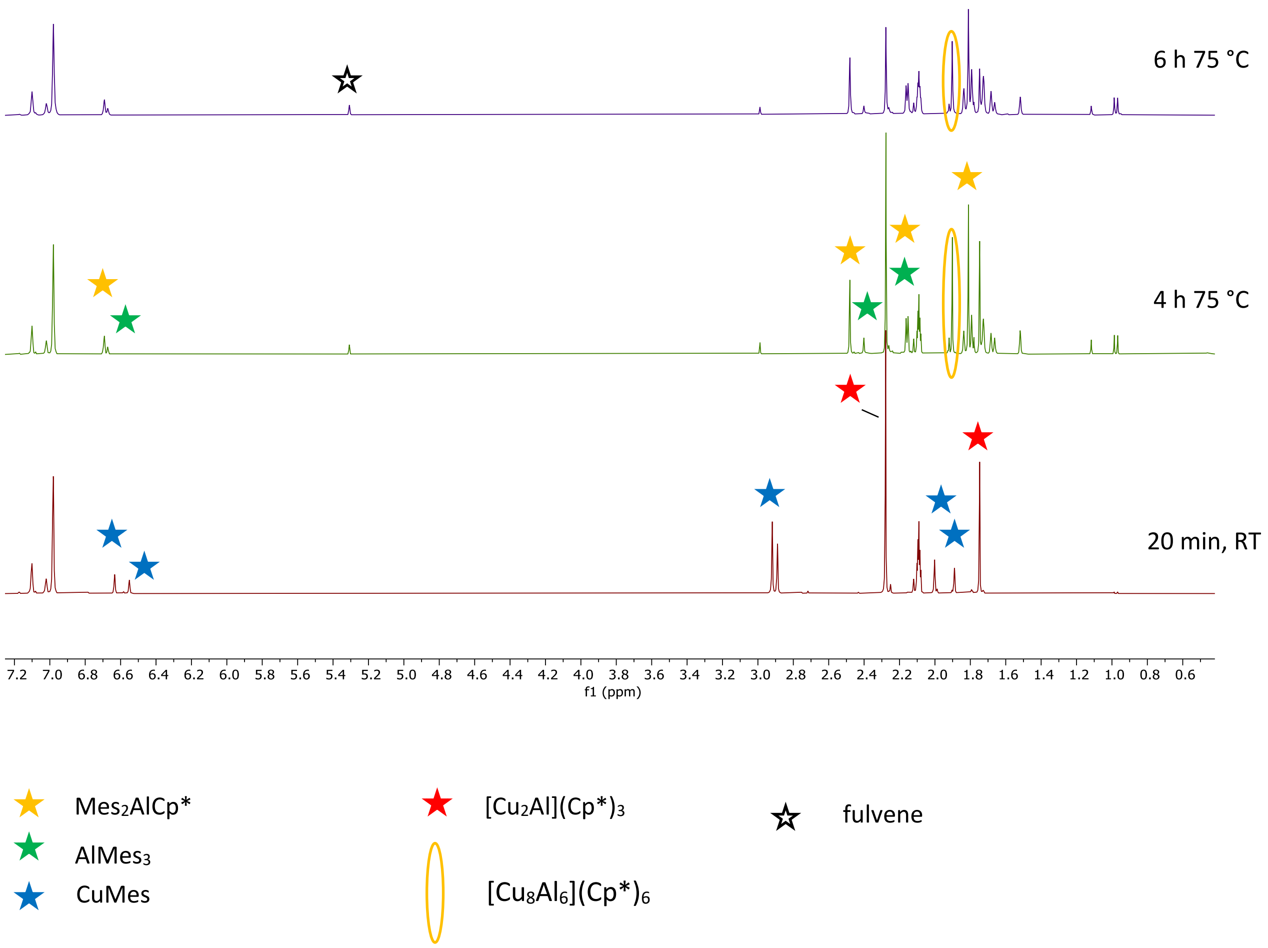

Figure S4: *In-situ* ^{1}H-NMR spectra (toluene-d_8) of the conversion of **2** with CuMes (1:1.2).

3. NMR analysis

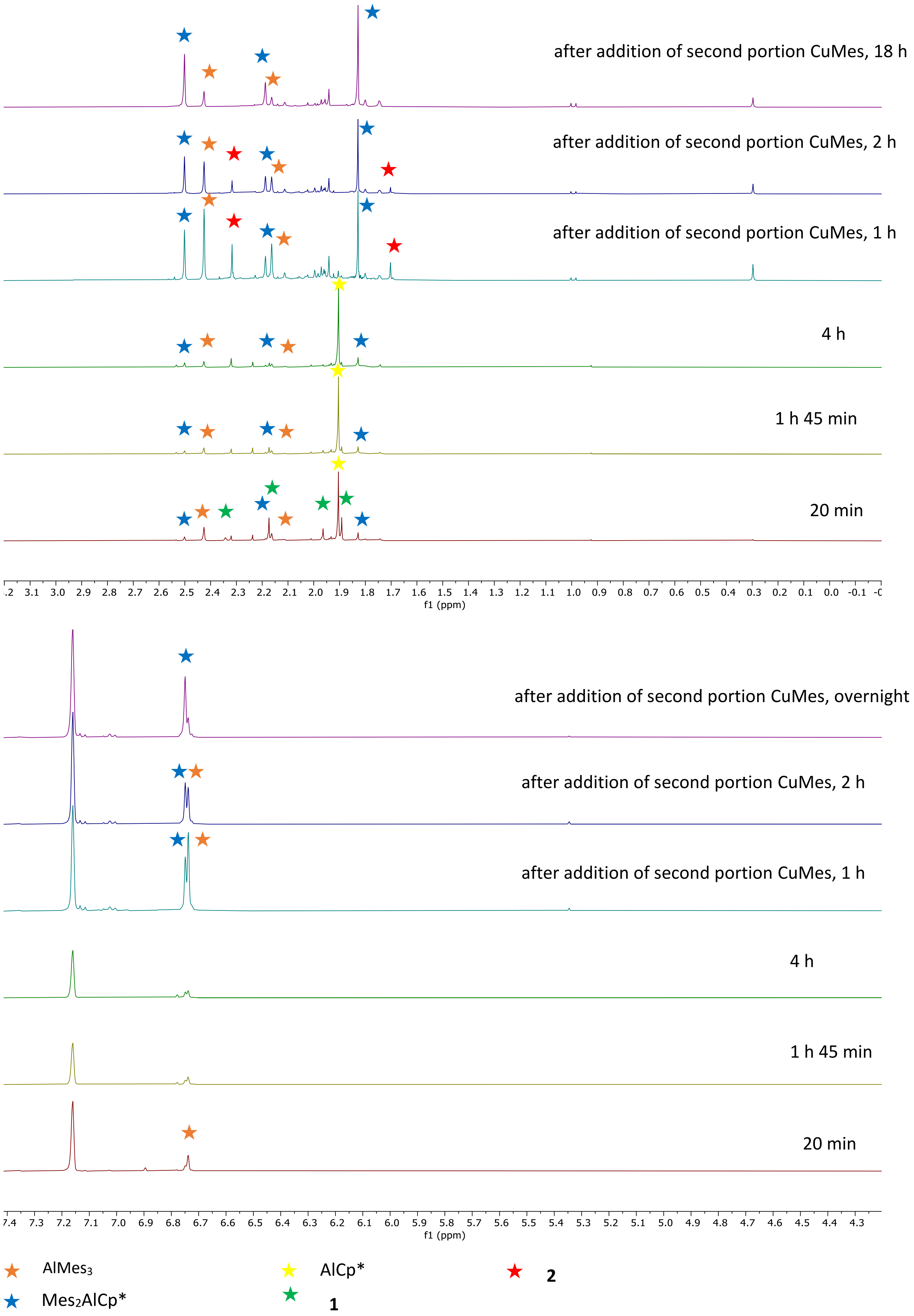

Figure S5: *In-situ* NMR spectra (benzene-d$_6$) of synthesis of **3/4**. The reaction was conducted at 75 °C.

3. NMR analysis

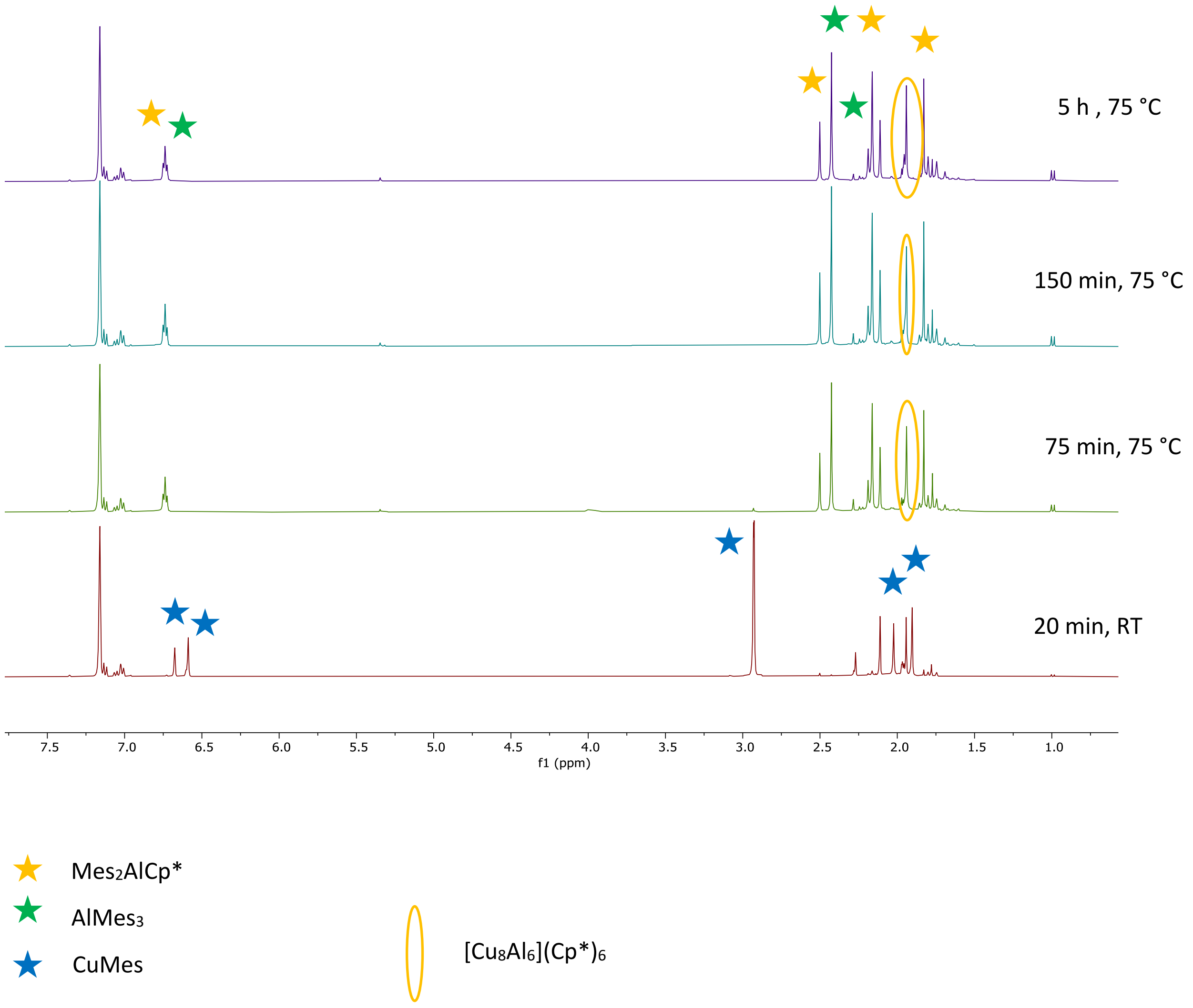

Figure S6: *In-situ* 1H-NMR spectra (benzene-d$_6$) of the conversion of **3/4** with CuMes (1:5).

3.2 Single point NMR analysis

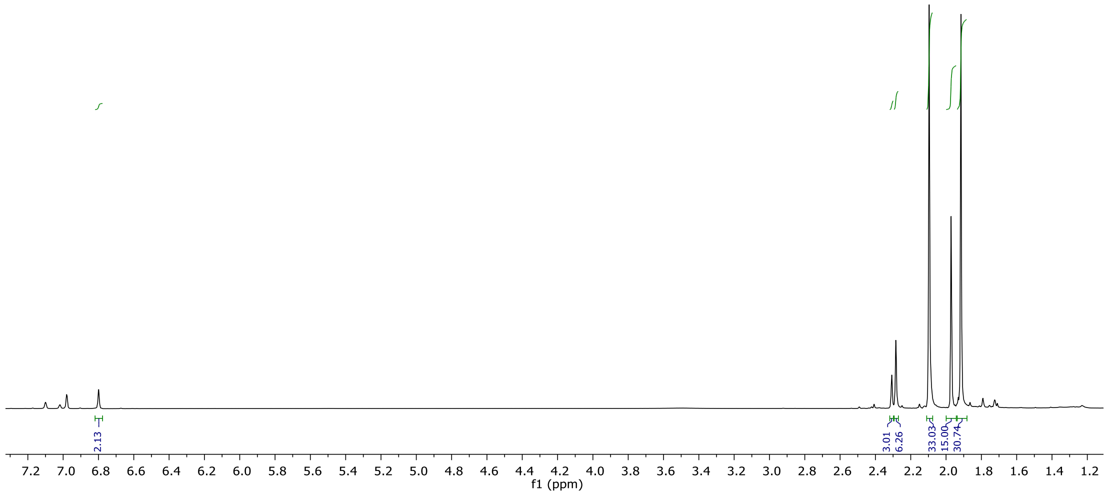

Figure S7: ^{1}H-NMR spectrum (toluene-d$_8$) of **1** in toluene-d$_8$ at room-temperature.

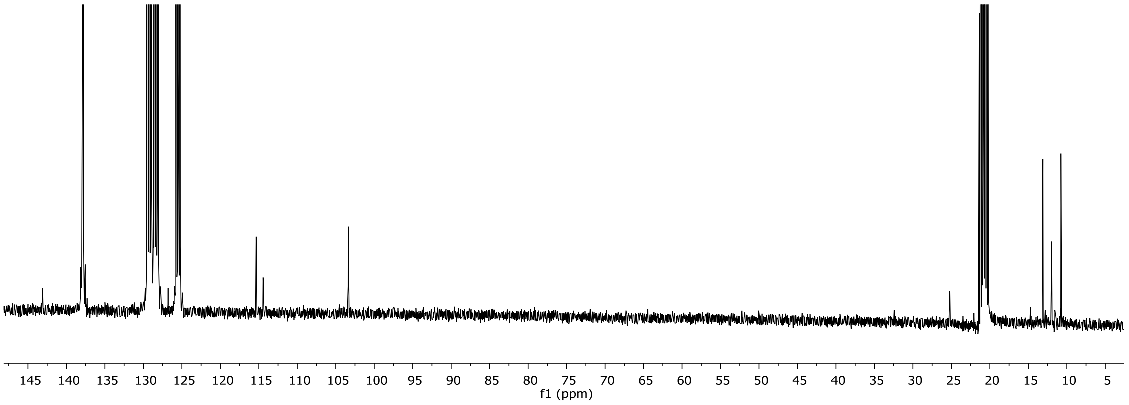

Figure S8: ^{13}C-NMR spectrum (toluene-d$_8$) of **1** at room-temperature.

The ^{1}H-NMR spectrum of ***1*** *in toluene-d^8 is fully consistent with the molecular symmetry found in the solid state. In the ^{13}C-NMR of* ***1*** *in toluene-d^8 all the expected signals were found apart from two aromatic mesityl carbon signals, which could not be identified due to small signal intensities. The ATR-IR spectrum shows the characteristic bands for the Cp* ligand as well as the characteristic ν_{Al-C} stretching vibration at 418.17 cm-1.[4] A band at 455 cm^{-1} is tentatively assigned to metal-metal vibrations within the cluster core. The elemental analysis of* ***1*** *is in good agreement with the calculated values.*

3. NMR analysis

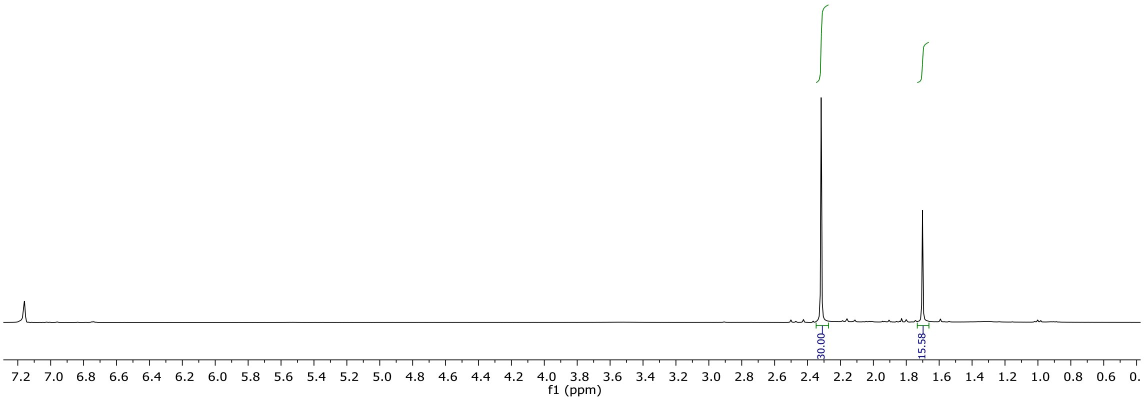

Figure S9: ^{1}H-NMR spectrum (benzene-d_6) of **2**.

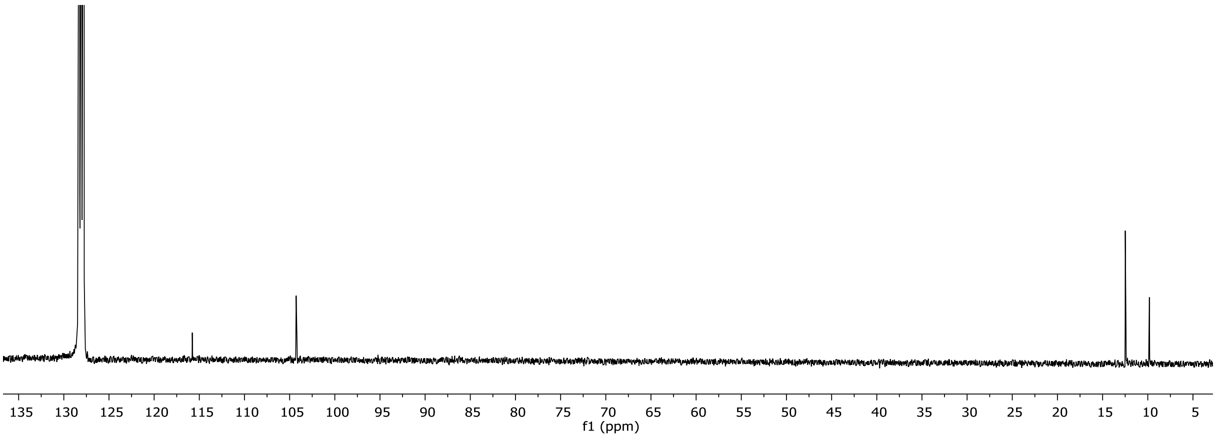

Figure S10: ^{13}C-NMR spectrum (benzene-d_6) of **2**.

The ^{1}H-NMR and ^{13}C-NMR spectrum of ***2*** *in benzene-d^6 show two sets of signals attributable to CuCp* and AlCp* moieties, fully consistent with the symmetry of the molecular structure in the solid state.*

3. NMR analysis

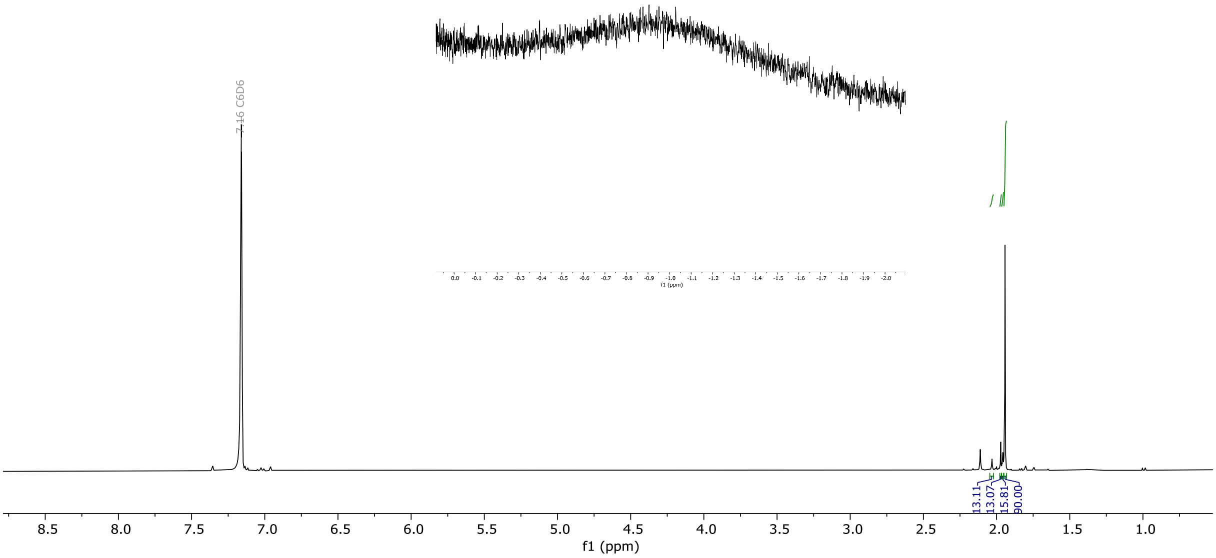

Figure S11: ^{1}H-NMR spectrum (benzene-d_6) of compound **3/4**. The inset shows the signal attributed to paramagnetic **3** at -0.95 ppm.

Note: Several small signals are observed at 2.03 ppm, 1.97 ppm and 1.95 ppm, probably assignable to minor quantities of smaller Cu/Al clusters also detected in LIFDI-MS spectra of the isolated product (see Figure S22). No significant spectral changes were observed in ^{1}H-NMR spectra recorded at variable temperature, however, with significant precipitation of the sample at low temperatures. The small peak at 2.11 ppm, as well as the aromatic signals at 6.9 ppm - 7.15 ppm are caused by toluene, which is co-crystallised with compound ***3.***

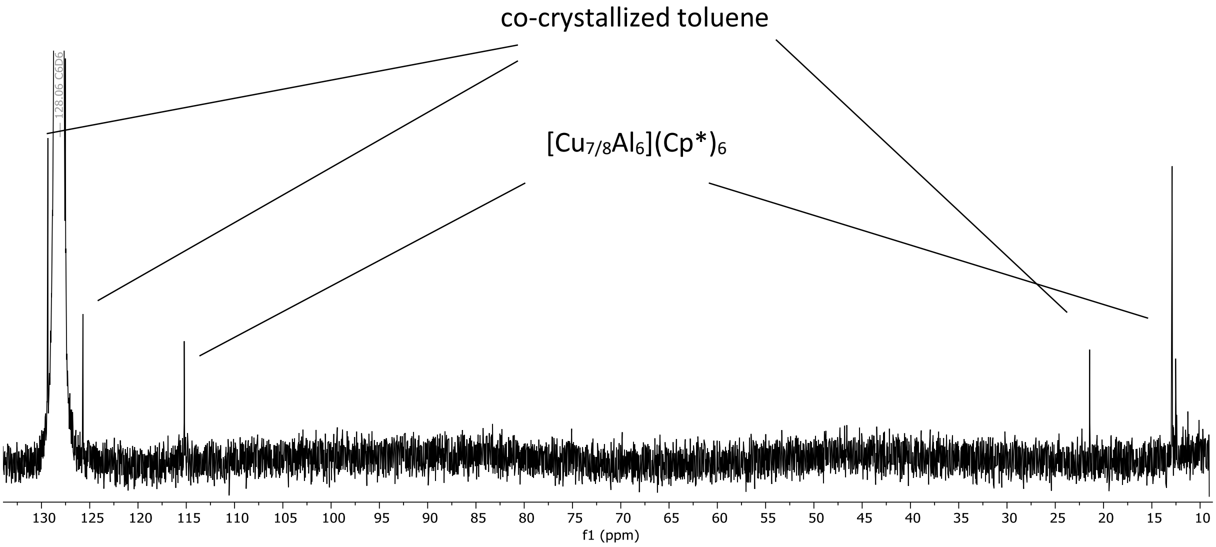

Figure S12: ^{13}C-NMR spectrum (benzene-d_6) of compound **3/4**.

3. NMR analysis

The ^{1}H-NMR of isolated ***3/4*** *in benzene-d^6 gives rise to one sharp singlet at 1.94 ppm, which is attributed to diamagnetic [Cu_8Al_6](Cp^*)$_6$. A very broad signal is observed at -1.03 ppm, which is assigned to paramagnetic [Cu_7Al_6](Cp^*)$_6$. The ^{13}C-NMR of* ***3/4*** *in benzene-d^6 shows signals for Cp* at 12.89 ppm and 115.19 ppm, again assigned to diamagnetic* ***4****, while paramagnetic* ***3*** *could not be identified in the ^{13}C-NMR spectrum.*

3. NMR analysis

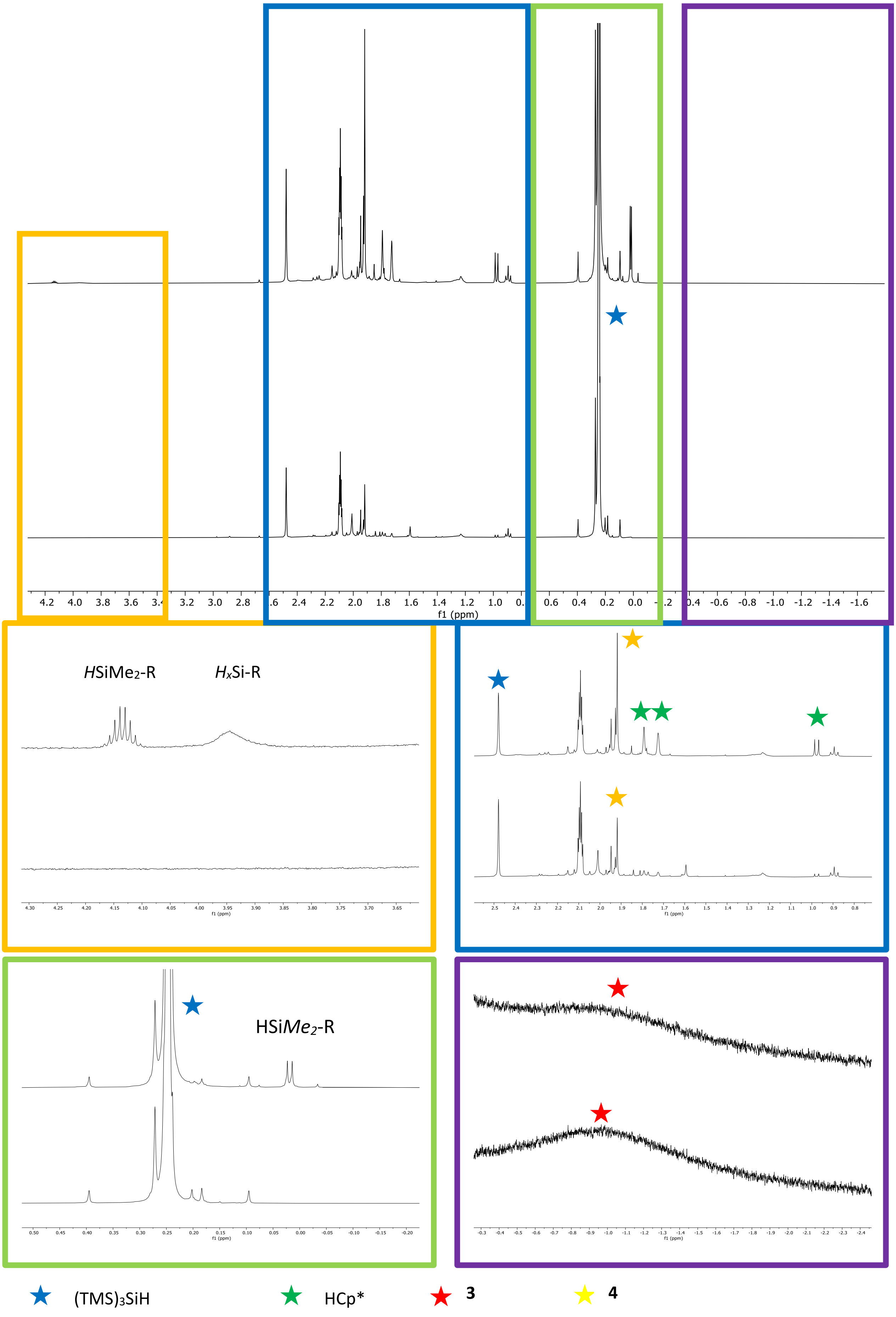

Figure S13: *In-situ* ^{1}H-NMR spectra (toluene-d$_8$) of the conversion of **3/4** with (TMS)$_3$SiH.

3. NMR analysis

Note: The silane reaction products could not unambiguously be identified by in-situ ^{1}H NMR spectroscopy. However, suggestions for functional groups of the species can be made and are inserted as text boxes in the spectra.[18] *It is noted that these suggestions are consistent with the GC-MS results. ^{29}Si spectra of the solution were recorded but due to low concentrations of the silane reaction products, no meaningful signals apart from unconsumed (TMS)$_3$SiH were observed.*

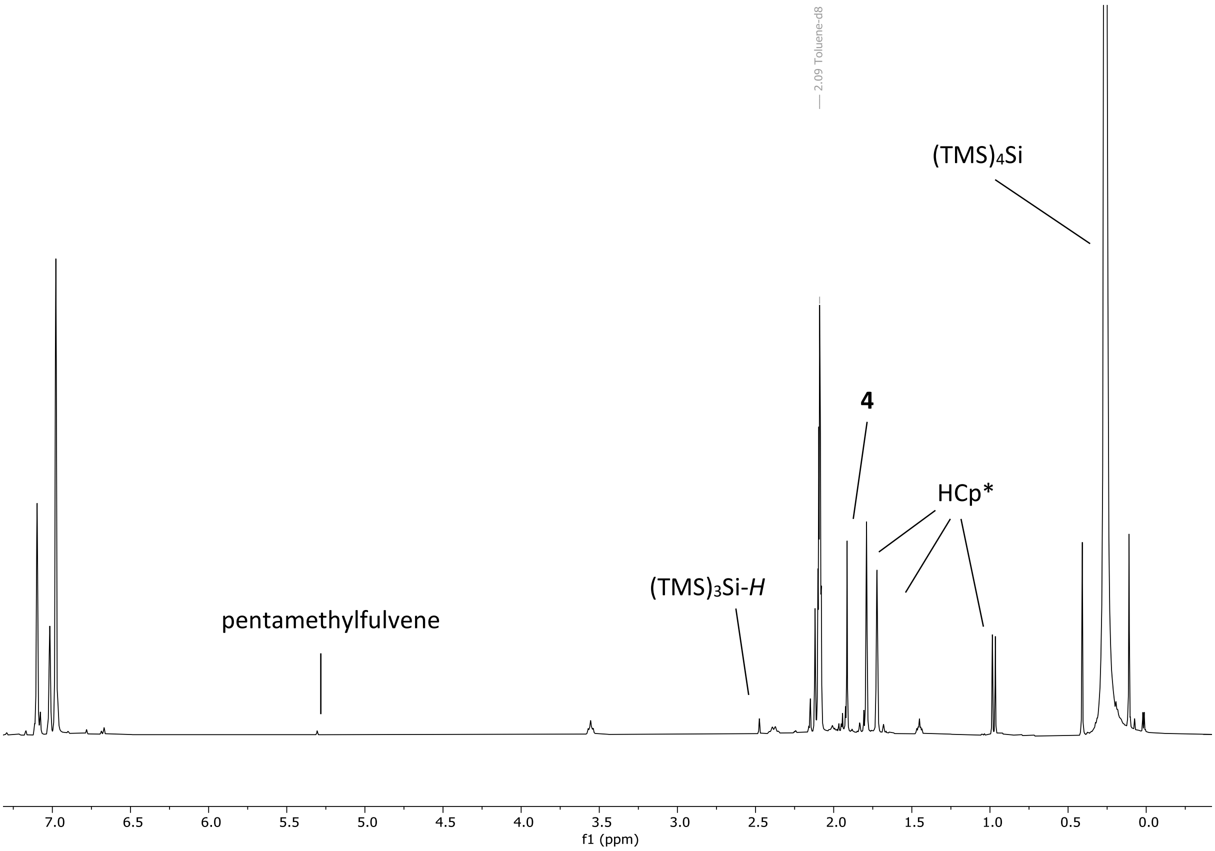

Figure S14: *In-situ* ^{1}H-NMR spectra (toluene-d$_8$, 110 °C, 5 days) of the conversion of **3/4** with (TMS)$_4$Si.

4. LIFDI-MS analysis

4.1 Time dependant LIFDI-MS analysis

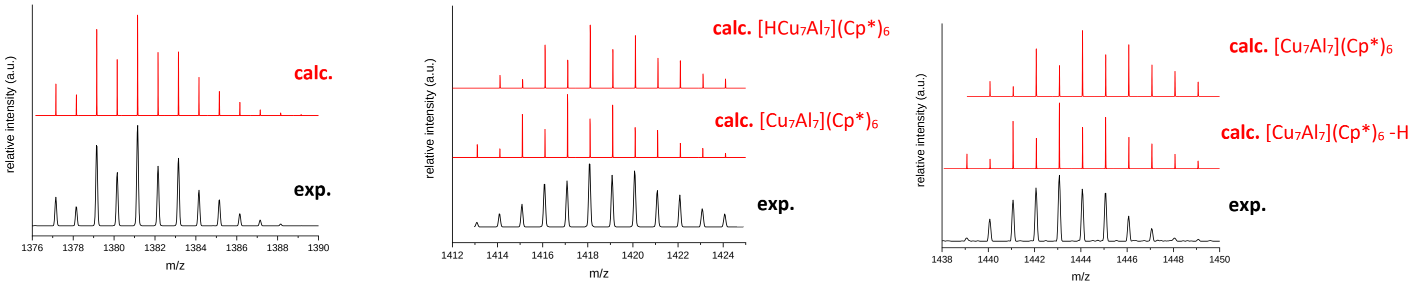

$[Cu_6Al_7](Cp^*)_6$

$[Cu_6Al_7](Cp^*)_6$ / $[HCu_7Al_7](Cp^*)_6$

$\{[Cu_7Al_7](Cp^*)_6\ \text{-H}\}$ / $[Cu_7Al_7](Cp^*)_6$

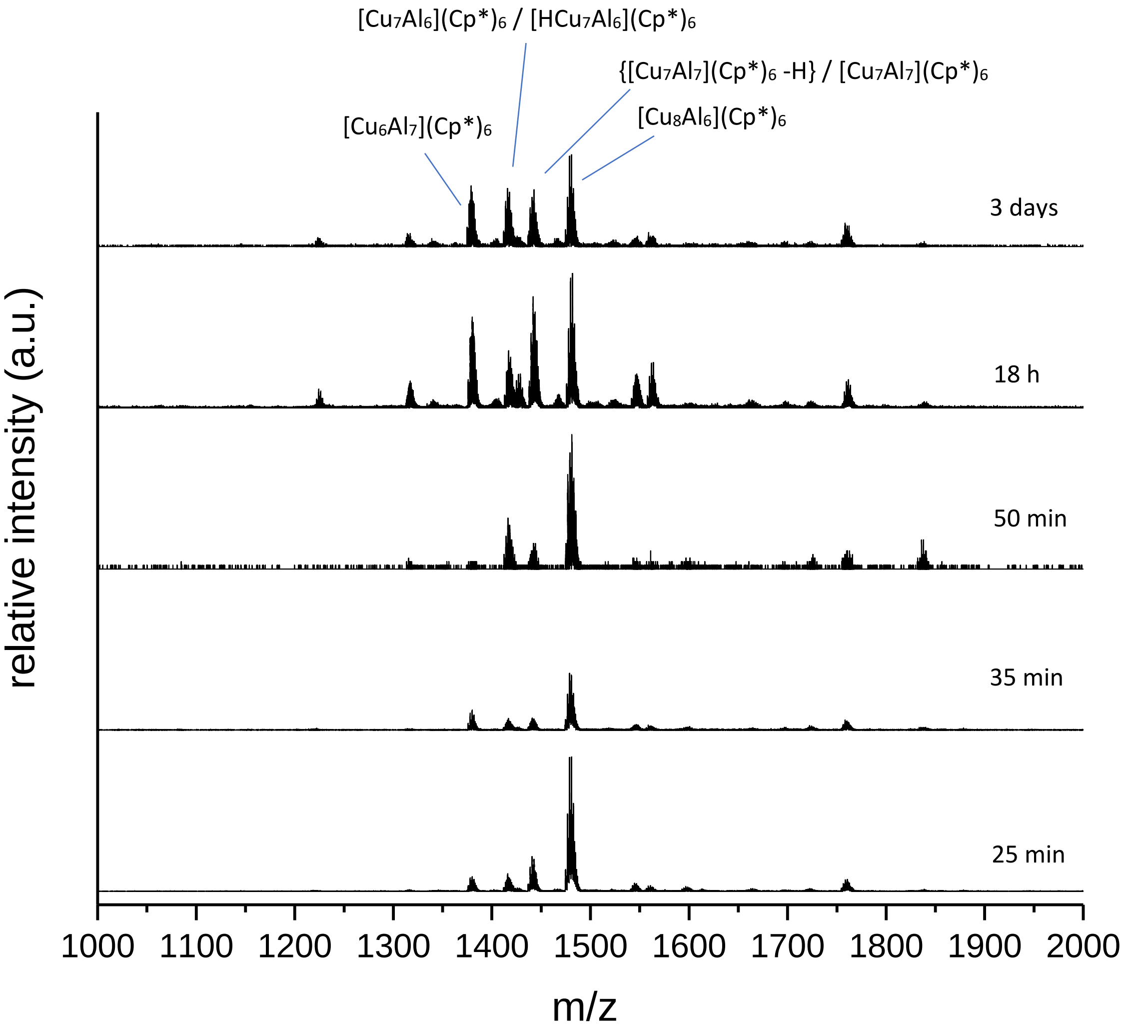

Figure S15: Bottom: LIFDI-MS spectra of the reaction solution CuMes + AlCp* (1:1.3, 75°C) after different reaction times. Top: Comparison between calculated (red) and experimental (black, determined by LIFDI-MS) mass-envelopes for the species $[Cu_6Al_7](Cp^*)_6$ and $\{[Cu_7Al_7](Cp^*)_6\ \text{-H}\}$. The Isotopic pattern of $[Cu_8Al_6](Cp^*)_6$ is depicted and analyzed in Figure S16.

4. LIFDI-MS analysis

Note: The peak at m/z = 1443 is found to be a mixture between the deprotonated cluster $[Cu_7Al_7](Cp^*)_6$ *-H and the parent ion* $[Cu_7Al_7](Cp^*)_6$*. Likewise, the peak at m/z = 1418 is a mixture between the radical* ***1*** *and the hydride* $\mathbf{1_H}$*.*

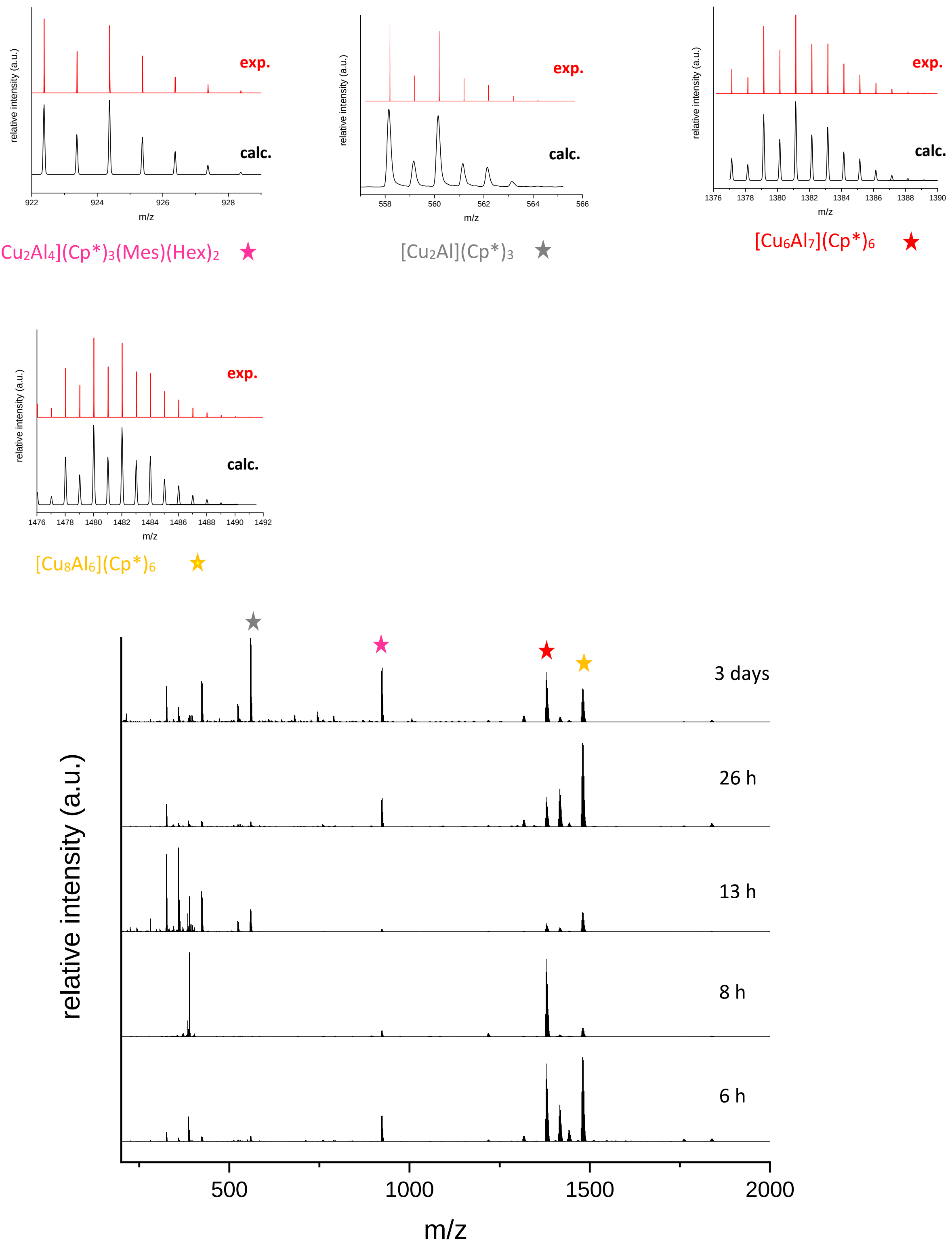

Figure S16: Bottom: Time-dependent LIFDI-MS spectra of the reaction solution **1** + 3-hexyne (10. Eq.), RT. Top: Enlarged isotopic pattern as determined by LIFDI-MS (red) and calculated mass envelopes (black) for selected peaks.

4. LIFDI-MS analysis

Table S2: Species observed in LIFDI-MS analysis of the reaction **1** + 3-hexyne (10 eq.), RT.

after 6 h	after 8 h	after 13 h	after 26 h	after 3 days
$[Cu_8Al_6](Cp^*)_6$	$[Cu_8Al_6](Cp^*)_6$	$[Cu_8Al_6](Cp^*)_6$	$[Cu_8Al_6](Cp^*)_6$	$[Cu_8Al_6](Cp^*)_6$
$[Cu_7Al_6](Cp^*)_6$	$[Cu_6Al_4](Cp^*)_3$	$[Cu_7Al_6](Cp^*)_6$	$[Cu_7Al_6](Cp^*)_6$	$H[Cu_7Al_6](Cp^*)_6$
$[Cu_7Al_6](Cp^*)_6(AntiH)_2$	$[Cu_7Al_7](Cp^*)_6(AntiH)$	$[Cu_7Al_7](Cp^*)_6(AntiH)$	$[Cu_7Al_7](Cp^*)_6(AntiH)$	$[Cu_7Al_7](Cp^*)_6(AntiH)$
$[Cu_8Al_6](Cp^*)_6(Mes)_3$	$[Cu_8Al_6](Cp^*)_6(Mes)_3$	$[Cu_8Al_6](Cp^*)_6(Mes)_3$	$[Cu_8Al_6](Cp^*)_6(Mes)_3$	$[Cu_8Al_6](Cp^*)_6(Mes)_3$
$[Cu_8Al_7](Cp^*)_7(Mes)(AntiH)$				
$[H_3Cu_3Al_2](Mes)(Hex)_2$ (small)		$[Cu_2Al](Cp^*)_2(Hex)$	$[H_3Cu_3Al_2](Mes)(Hex)_2$	$[Cu_3Al_5](Cp^*)_2(Hex)_5$
			$[Cu_3Al_2](Cp^*)(Mes)(Hex)_3$	$[Cu_3Al_2](Cp^*)(Mes)(Hex)_3$
				$[Cu_5Al_2](Cp^*)(Mes)(Hex)_4$
				$[Cu_5Al_2](Cp^*)(Mes)(Hex)_3$
$[Cu_6Al_6](Cp^*)_5$	$[Cu_6Al_6](Cp^*)_5$	$[Cu_6Al_6](Cp^*)_5$	$[Cu_6Al_6](Cp^*)_5$	$[Cu_6Al_6](Cp^*)_5$
$[HCuAl_4](Cp^*)(Hex)$		$[CuAl_4](Cp^*)_2(Hex)$	$[CuAl_4](Cp^*)_2(Hex)$	$[H_4CuAl_3](Cp^*)_3$
$[Cu_2Al_3](Cp^*)_3(Hex)(H)_2$	$[Cu_2Al_3](Mes)_2(Hex)(H)_2$		$[H_2Cu_2Al_3](Cp^*)_3(Hex)$	
$[Cu_2Al_3](Cp^*)_2(Mes)(Hex)$	$[Cu_2Al_3](Cp^*)_2(Mes)(Hex)_2$		$[Cu_2Al_3](Cp^*)_2(Mes)$	
			$[H_4CuAl_3](Cp^*)_3$	$[H_4CuAl_3](Cp^*)_3$
			$[H_4Cu_2Al_5](Hex)_3$	
$[Cu_2Al_4](Cp^*)_3(Mes)(Hex)_2$	$[Cu_2Al_4](Cp^*)_3(Mes)(Hex)_2$	$[Cu_2Al_4](Cp^*)_3(Mes)(Hex)_2$	$[Cu_2Al_4](Cp^*)_3(Mes)(Hex)_2$	$[Cu_2Al_4](Cp^*)_3(Mes)(Hex)_2$
$[Cu_2Al_4](Cp^*)_2(Mes)(Hex)_2$				$[HCu_2Al_4](Cp^*)_2(Mes)(Hex)_2$
$[Cu_2Al_4](Cp^*)_3(Mes)(Hex)$			$[Cu_2Al_4](Cp^*)_3(Mes)(Hex)$	$[Cu_2Al_4](Cp^*)_3(Mes)(Hex)$
$[Cu_2Al_4](Cp^*)_2(Mes)_2(Hex)_2$				$[Cu_2Al_2](Cp^*)(Mes)(Hex)_3$
$[Cu_2Al_4](Cp^*)_2(Mes)(Hex)$			$[Cu_2Al_4](Cp^*)_2(Mes)(Hex)$	
$[HCu_2Al_4](Cp^*)_2(Mes)(Hex)_3$				
$[Cu_5Al_7](Cp^*)_6$	$[Cu_5Al_7](Cp^*)_6$	$[Cu_5Al_7](Cp^*)_6$	$[Cu_5Al_7](Cp^*)_6$	$[Cu_5Al_7](Cp^*)_6$
			$[Cu_3Al_5](Cp^*)_2(Hex)_5$	$[Cu_4Al_6](Cp^*)_2(Hex)_6$
$[H_4Cu_5Al_{19}](Hex)_9$ (small)			$[HCu_2Al_6](Cp^*)_3(Hex)$	$[Cu_2Al_5](Cp^*)_3(Hex)_4$
$[Cu_6Al_8](Mes)_3(Hex)_4$			$[H_4Cu_5Al_{19}](Hex)_9$ (small)	$[HCu_3Al_8](Cp^*)(Mes)(Hex)_6$
$[Cu_5Al_{16}](Cp^*)(Mes)_2(Hex)_6$				
$[Cu_6Al_7](Cp^*)_6$	$[Cu_6Al_7](Cp^*)_6$	$[Cu_6Al_7](Cp^*)_6$	$[Cu_6Al_7](Cp^*)_6$	$[Cu_6Al_7](Cp^*)_6$
$[Cu_2Al](Cp^*)_3$		$[Cu_2Al](Cp^*)_3$	$[Cu_2Al](Cp^*)_3$	
$[Cu_2Al](Cp^*)_2$		$[Cu_2Al](Cp^*)_2$	$[Cu_2Al](Cp^*)_2$	
$[Cu](Cp^*)_2$			$[Cu](Cp^*)_2$	$[Cu_2](Cp^*)_2$
				$[HCu_2Al](Cp^*)_2(Mes)$

yellow: Cu-rich clusters; blue: Cu:Al 1:1 clusters; green: small, Cu-rich clusters; light green: Al-rich coordination compound; blue / pink: Al rich-clusters, $[Cu_2Al_4](Cp^*)_3(Mes)(Hex)$ = main side product; red: large, Al-rich clusters; grey: 2 and fragments thereof;

Note: Isotopic patterns of the main peaks in LIFDI-MS spectra of reaction solutions (3 days) are shown in Figure S16, top.

4. LIFDI-MS analysis

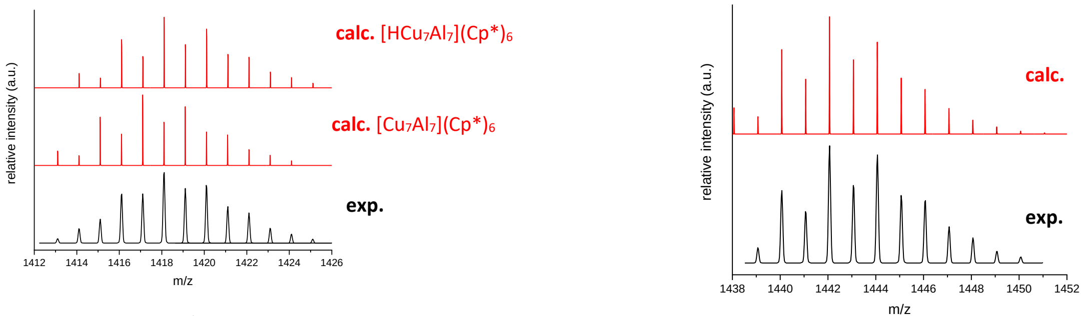

$[HCu_7Al_6](Cp^*)_6$ / $[Cu_7Al_6](Cp^*)_6$

$\{[Cu_7Al_7](Cp^*)_6 – 2H\}$

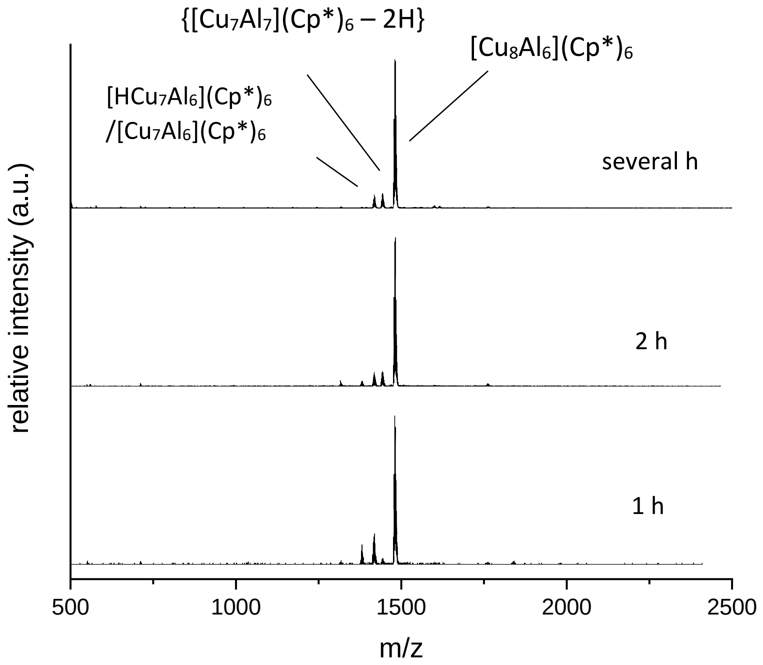

Figure S17: Bottom: LIFDI-MS spectra of a solution of isolated $[Cu_4Al_4](Cp^*)_5(Mes)$ (**1**) in toluene heated to 75 °C. Top: Comparison between experimental (black, LFIDI-MS) and calculated (red) isotopic patterns for selected peaks.

Note: The isotopic pattern of $[Cu_8Al_6](Cp^*)_6$ *is shown in Figure S16.*

4. LIFDI-MS analysis

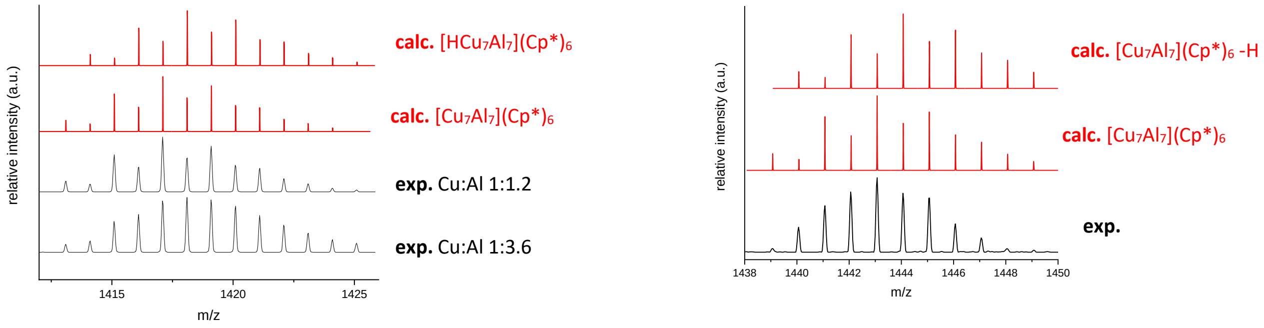

$[Cu_7Al_6](Cp^*)_6$

$\{[Cu_7Al_7](Cp^*)_6\ \text{-H}\} / [Cu_7Al_7](Cp^*)_6$

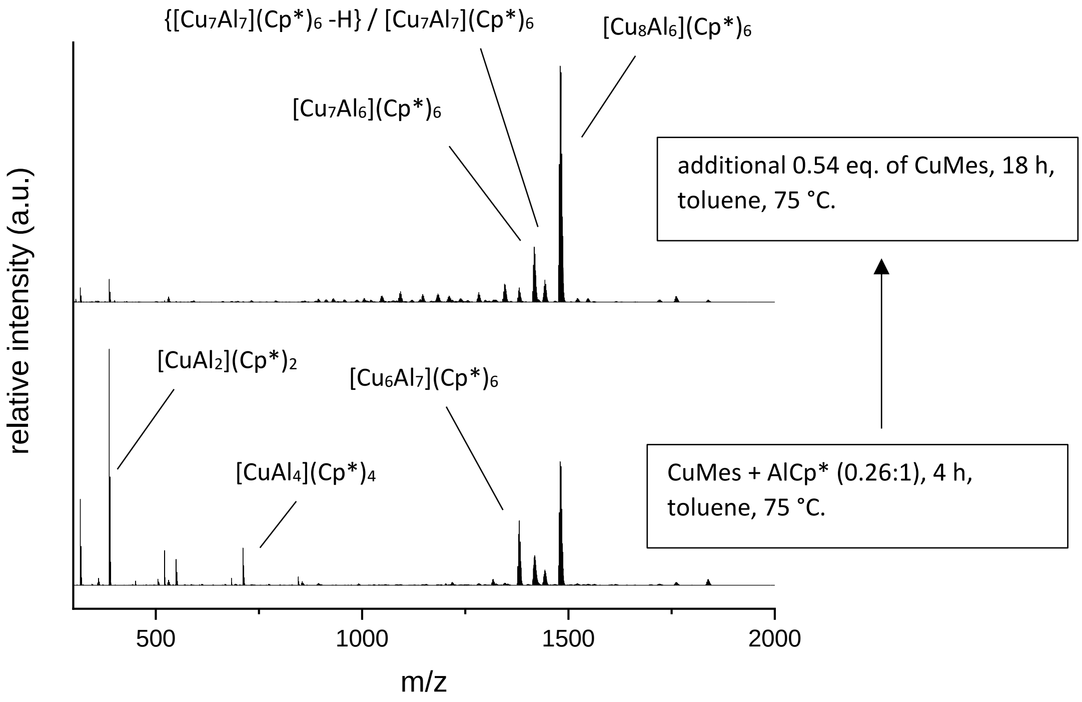

Figure S18: Bottom: *In situ* LIFDI-MS spectra of the synthesis of **3**/**4**. Top: Comparison between experimental (black, LIFDI-MS) and calculated (red) isotopic pattern for **3** and $\{[Cu_6Al_7](Cp^*)_6 - H\}$.

*Note: Figure S20 (top, left) illustrates the size-focusing process towards the radical species **3**. Before addition of the second portion of CuMes, a mixture between **3** and **3**$_H$ is detected, which is converted to pure **3** upon CuMes addition. For isotopic patterns of $[Cu_6Al_7](Cp^*)_6$ and $[Cu_8Al_6](Cp^*)_6$ see Figure S16.*

4. LIFDI-MS analysis

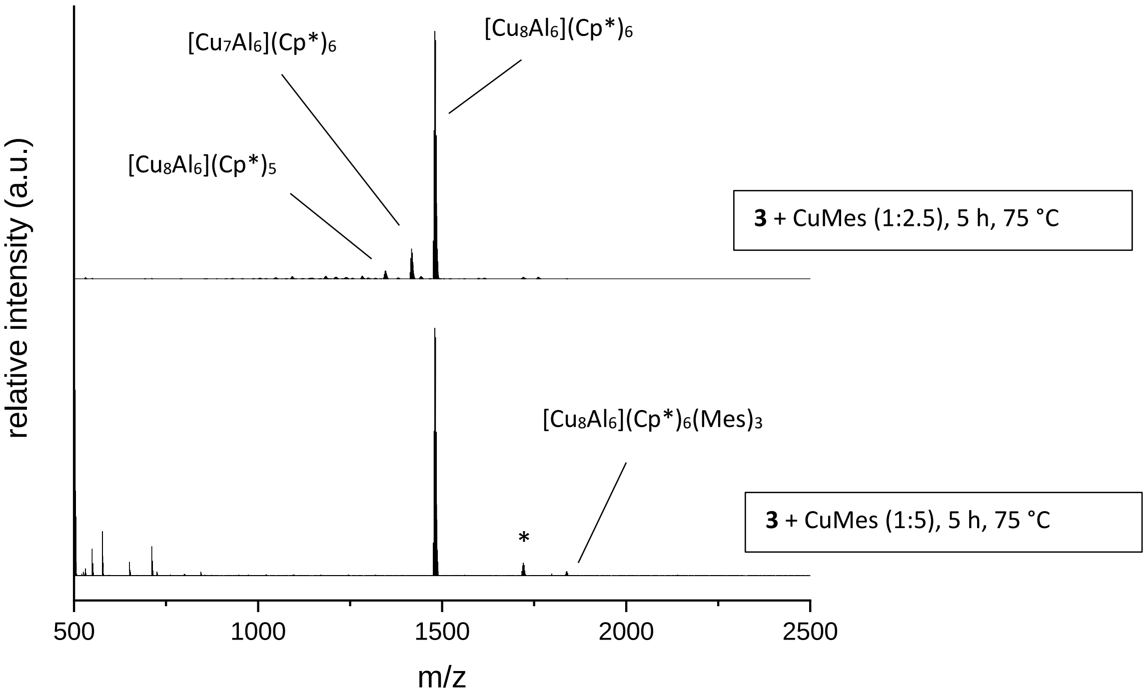

Figure S19: *In-situ* LIFDI-MS spectra of the reaction of **3/4** with CuMes: Bottom: Conversion with 5 eq. CuMes, toluene, 75 °C, 5h; Top: Conversion with 2.5 eq. CuMes, toluene, 75 °C, 5 h.

** Note: The small peak at m/z = 1720 in the lower spectrum is attributed to $[Cu_8Al_6](Cp^*)_6(Br)_3$ and caused by trace impurities of bromide in CuMes. Due to its very low intensity it can be assumed that the small impurities do not affect the general outcome of the reactions studied.*

4.2 Single point LIFDI-MS analysis

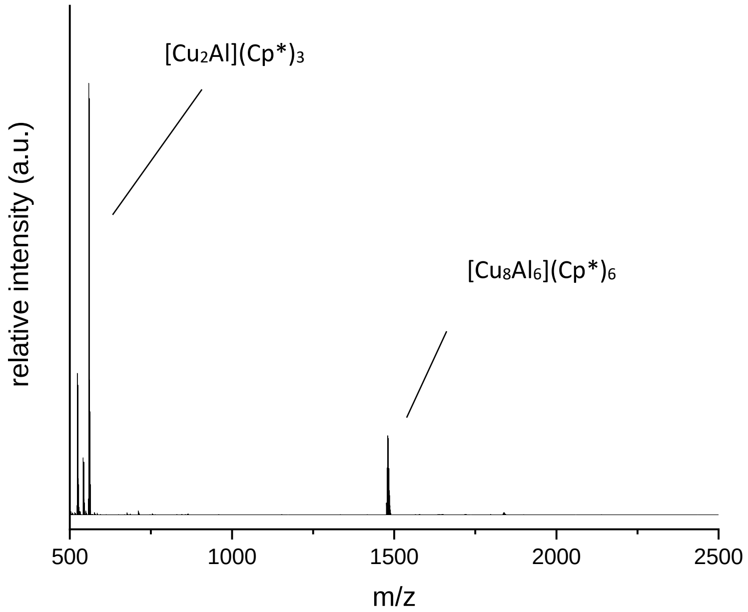

Figure S20: *In-situ* LIFDI-MS spectra of the conversion of **2** with CuMes (1:1.2, toluene, 75°C, 7 h).

4. LIFDI-MS analysis

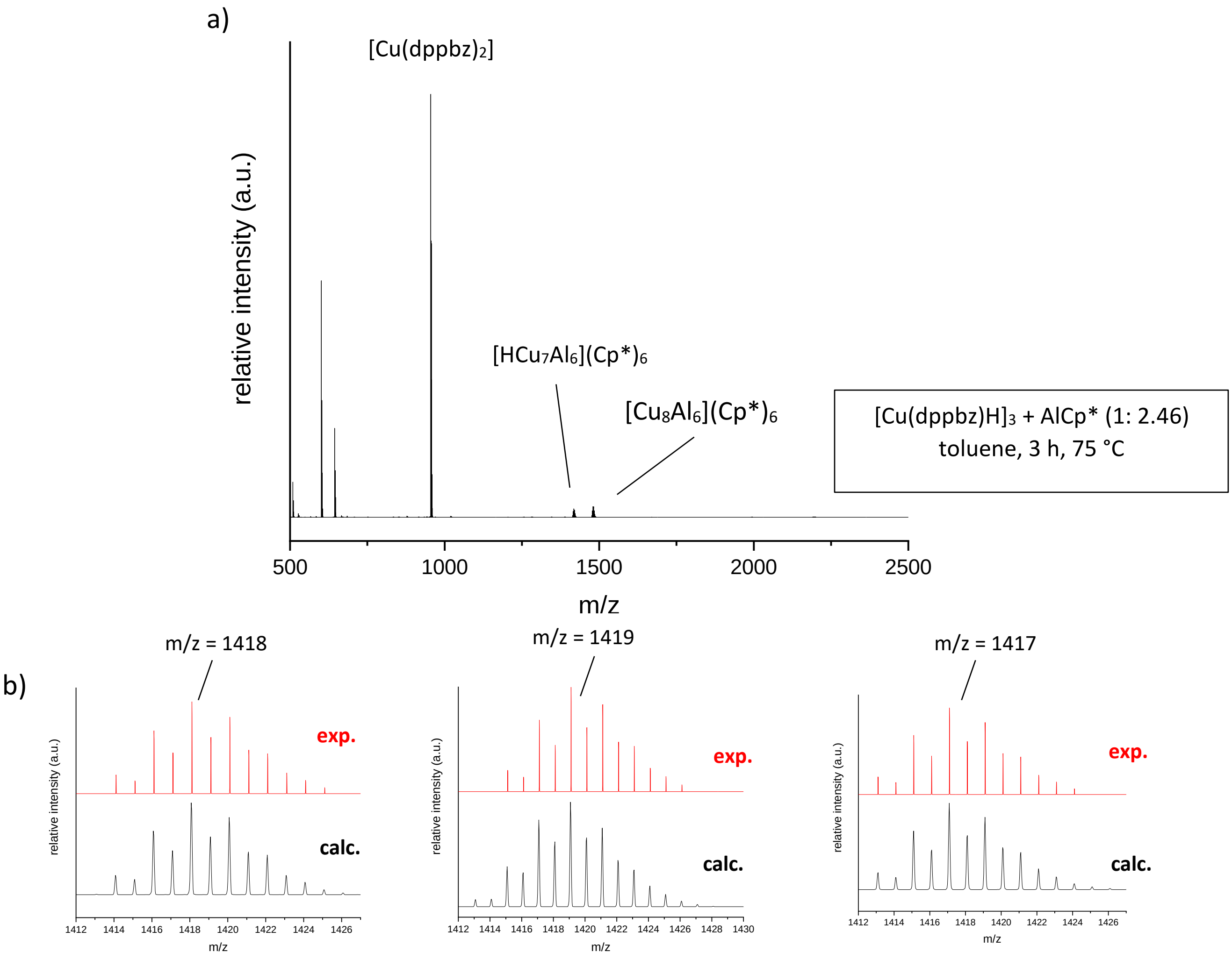

3$_H$

from [Cu(dppbz)H]$_3$

3$_D$

from [Cu(dppbz)D]$_3$

3

from CuMes + AlCp*

Figure S21: a) Full range LIFDI-MS spectrum of the reaction solution [Cu(dppbz)H]$_3$ + AlCp* (1: 2.46, toluene, 3 h, 75 °C). b) Comparison of experimental (black, LIFDI-MS) and calculated mass envelopes (red) of the species **3$_H$**, **3$_D$** and **3**.

4. LIFDI-MS analysis

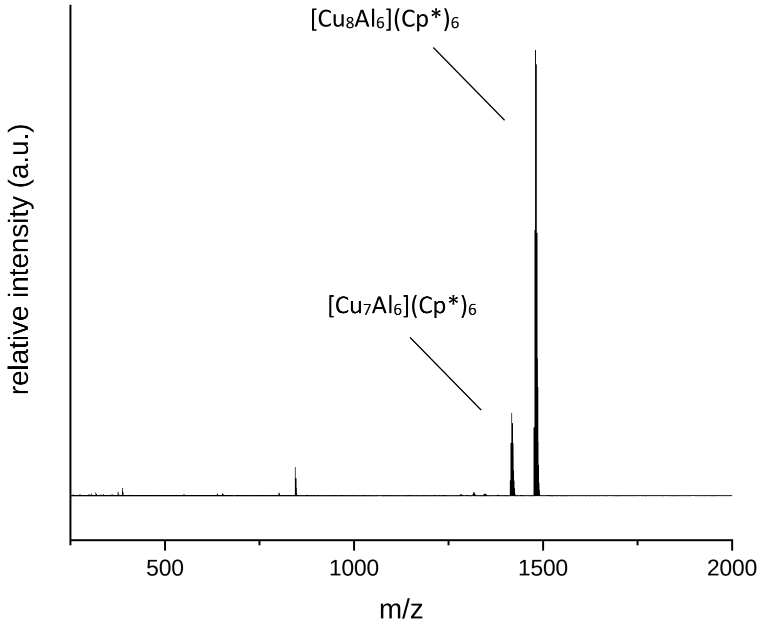

Figure S22: LIFDI-MS spectrum of isolated compound **3/4**. For isotopic pattern assignment see Figure S21 for **3**, as well as Figure 4 (main article) for **4**.

Note: Small signals of other Cu/Al clusters are observed in the full-range spectrum of isolated ***3/4*** *highlighting the difficulty of separation of closely related cluster species. Isotopic pattern analysis for both* ***3*** *and* ***4*** *is presented in the main article and in Figures S21 and S16, respectively.*

4. LIFDI-MS analysis

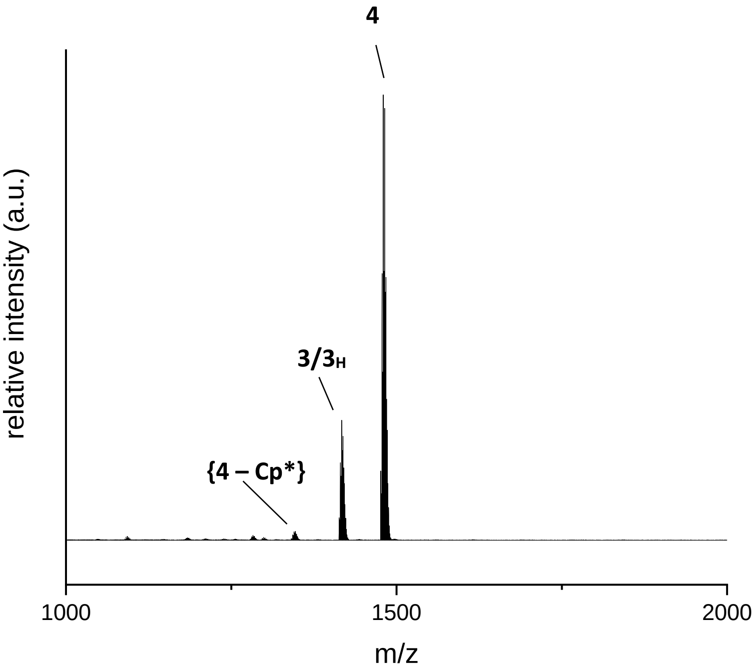

Figure S23: Full range *in-situ* LIFDI-MS spectrum of a solution of **3/4** heated in toluene-h_8 to 110 °C for 5 days.

4. LIFDI-MS analysis

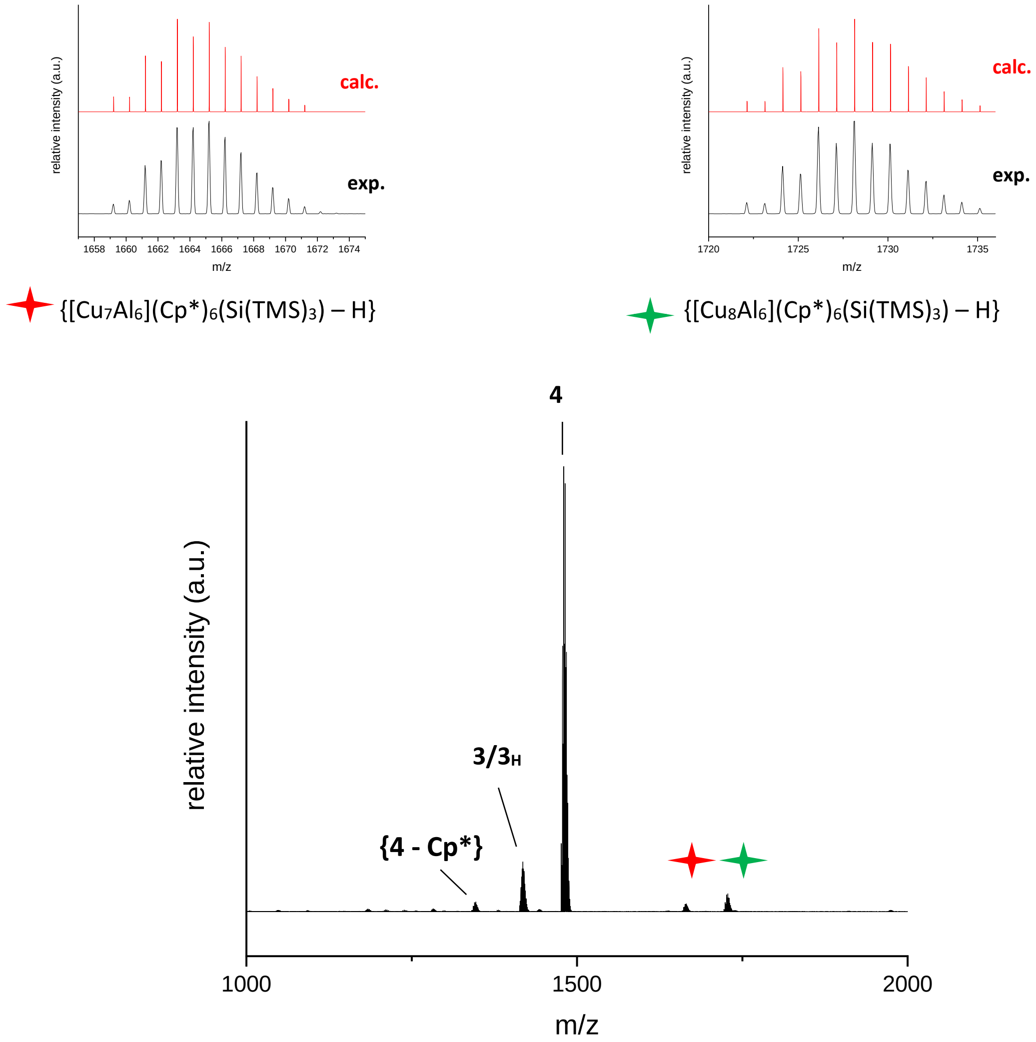

Figure S24: *In-situ* LIFDI-MS spectrum of the conversion of **3/4** with (TMS)$_3$SiH (toluene-h$_8$, 110 °C, 5 days).

4. LIFDI-MS analysis

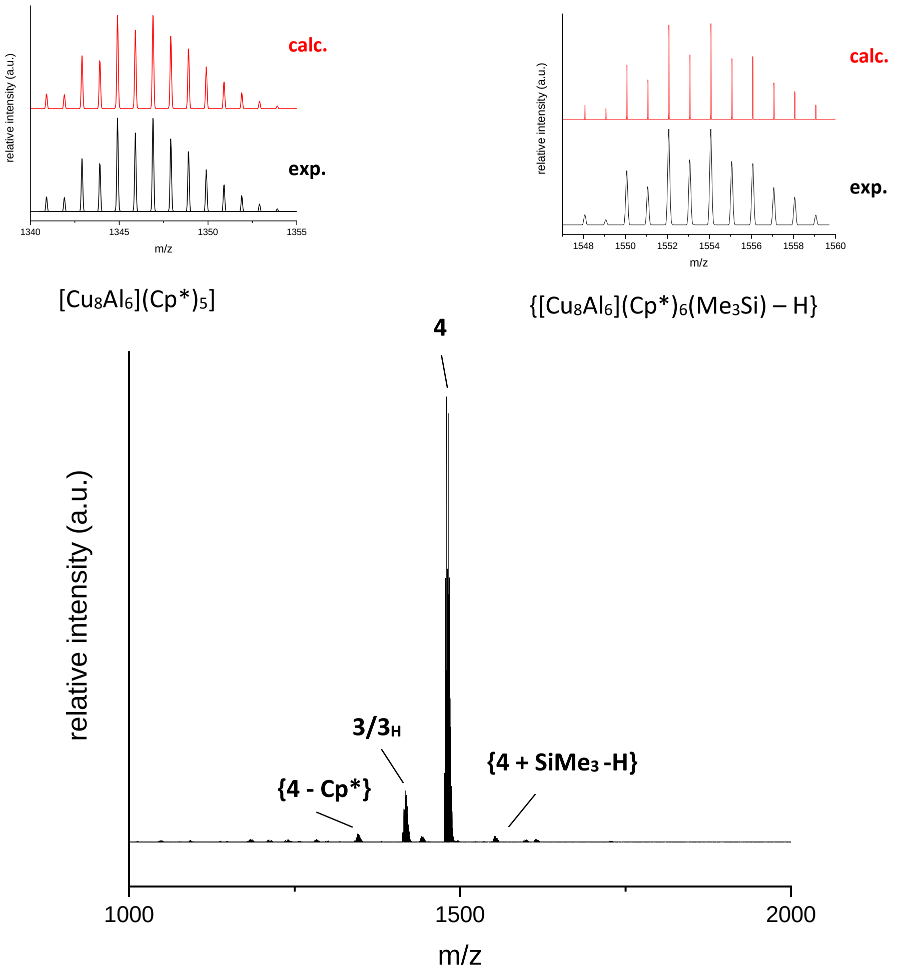

Figure S25: *In-situ* LIFDI-MS spectrum of the conversion of **3/4** with (TMS)$_4$Si (toluene, 110 °C, 5 days).

Note: Whether [Cu$_8$Al$_6$](Cp)$_5$ is also formed as a product of the reaction with toluene or is only fragment of **4** is unclear so far and will be subject of further investigations.*

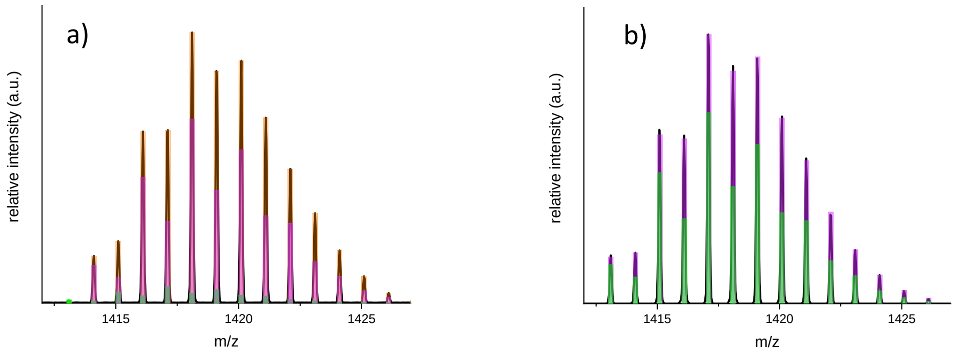

Figure S26: a) Isotopic pattern of a mixture of **3**/**3$_H$**/**3$_D$** as determined by LIFDI-MS after heating of **3** with excess (TMS)$_3$SiD in toluene (110 °C, 5 days). Fractions of **3**, **3$_H$** and **3$_D$** are illustrated in green, purple and orange, respectively. b) Isotopic pattern of a mixture of **3**/**3$_H$** as determined by LIFDI-MS after heating of **3** with excess (TMS)$_4$Si in toluene (110 °C, 5 days). Fractions of **3** and **3$_H$** are illustrated in green and purple, respectively.

4. LIFDI-MS analysis

*Note: The presented figures show deconvolution of the detected peak into its components (**3**, **3_H**, **3_D**). The calculated isotopic patterns of **3**, **3_H** and **3_D** are shown in Figure S23.*

Table S3: LIFDI-MS data (peak centers with corresponding intensity, normalized to the highest peak in the pattern) for the most important species described in this work.

$[Cu_8Al_6](Cp^*)_6$ (4)		**$\{[Cu_7Al_6](Cp^*)_6$ + $(TMS)_3Si – H\}$**		**3/4** + $(TMS)_3SiH$, tol-h_8	
m/z	*I*	*m/z*	*I*	*m/z*	*I*
1476,0303	0,61664	1659,19855	0,1045	1413,08125	0,01352
1477,0303	0,59425	1660,19265	0,14578	1414,0895	0,02368
1478,0303	0,81562	1661,18765	0,52092	1415,09883	0,05429
1479,0303	0,72252	1662,18354	0,57442	1416,08397	0,07839
1480,0303	1	1663,18032	0,92898	1417,09544	0,09631
1481,0303	0,82871	1664,2102	0,93102	1418,08266	0,11176
1482,0303	0,99118	1665,20881	1	1419,09628	0,09633
1483,0303	0,8065	1666,20832	0,82685	1420,08559	0,09082
1484,0303	0,82604	1667,20873	0,66084	1421,07595	0,06184
1485,0303	0,69777	1668,21004	0,44164	1422,09277	0,04667
1486,0225	0,66349	1669,17991	0,28368	1423,08522	0,029
1487,0225	0,60355	1670,183	0,16524	1424,07871	0,01644
1488,0225	0,57875	1671,18699	0,07736	1425,07325	0,00926
				1426,09436	0,00416
				1427,09101	0,00247
$[Cu_7Al_6](Cp^*)_6$ (3)		**$\{[Cu_8Al_6](Cp^*)_6$ +$(TMS)_3Si – H\}$**		**3/4** + $(TMS)_3SiH$, tol-h_8	
m/z	*I*	*m/z*	*I*	*m/z*	*I*
1413,10327	0,19646	1722,12354	0,12115	1413,08864	0,17432
1414,08632	0,14047	1723,14081	0,11189	1414,0969	0,18807
1415,09565	0,67786	1724,12503	0,51267	1415,08099	0,63728
1416,10606	0,45779	1725,11009	0,42951	1416,09138	0,62826
1417,09224	1	1726,13001	0,93643	1417,07755	1
1418,10479	0,62481	1727,11679	0,76039	1418,09008	0,88068
1419,09307	0,83636	1728,13849	1	1419,07835	0,91483
1420,08238	0,48773	1729,127	0,76327	1420,09302	0,68191
1421,09813	0,43038	1730,11635	0,75356	1421,08338	0,53428
1422,08954	0,2407	1731,10655	0,47251	1422,07477	0,33678
1423,08198	0,14736	1732,13179	0,35154	1423,09267	0,19423
1424,10096	0,06835	1733,12373	0,20414	1424,08616	0,10776
1425,09551	0,03282	1734,11651	0,1262	1425,0807	0,05053
1426,09111	0,01284			1426,07628	0,02121
1427,08774	0,00456				

4. LIFDI-MS analysis

[HCu$_7$Al$_6$]Cp*$_6$ (3$_{\mathrm{H}}$)		**{[Cu$_8$Al$_6$]Cp*$_6$ + Me$_3$Si -H}**		**3/4** + (TMS)$_4$Si	
m/z	*I*	*m/z*	*I*	*m/z*	*I*
1414,08014	0,21084	1548,07009	0,10807	1413,09703	0,17915
1415,08946	0,16639	1549,05272	0,05391	1414,10528	0,18912
1416,07459	0,69378	1550,06523	0,56494	1415,08936	0,64567
1417,08605	0,47913	1551,04976	0,39716	1416,09975	0,62437
1418,07326	1	1552,06423	0,99927	1417,08592	1
1419,08686	0,63002	1553,05067	0,67853	1418,09844	0,88313
1420,07617	0,84121	1554,0671	1	1419,0867	0,91114
1421,09192	0,46501	1555,05545	0,66206	1420,10137	0,69533
1422,08333	0,43252	1556,07385	0,63931	1421,09172	0,53933
1423,07577	0,21039	1557,06411	0,38966	1422,08311	0,3305
1424,06925	0,13646	1558,05532	0,28825	1423,10099	0,19916
1425,06377	0,05451	1559,04747	0,10327	1424,09448	0,10619
1426,08488	0,01898			1425,08901	0,04695
				1426,08459	0,01712

[DCu$_7$Al$_6$]Cp*$_6$ (3$_{\mathrm{D}}$)		**3/4** + tol-h$_8$		**3/4** + tol-d$_8$	
m/z	*I*	*m/z*	*I*	*m/z*	*I*
1413,09104	0,06756	1413,09144	0,05343	1413,08333	0,18758
1414,07407	0,07223	1414,09969	0,18608	1414,09158	0,16787
1415,08338	0,3836	1415,10902	0,29016	1415,10091	0,64577
1416,09377	0,32524	1416,09416	0,61637	1416,08605	0,53354
1417,07994	0,8303	1417,10563	0,61166	1417,09752	1
1418,09247	0,62086	1418,09285	0,8872	1418,08474	0,74638
1419,08074	1	1419,10647	0,67662	1419,09835	0,86672
1420,09541	0,65894	1420,09578	0,7394	1420,08766	0,60307
1421,08577	0,7525	1421,11154	0,43989	1421,07801	0,47266
1422,07716	0,44337	1422,10296	0,37648	1422,09483	0,29692
1423,09505	0,35139	1423,09541	0,19276	1423,08728	0,1824
1424,08855	0,19799	1424,0889	0,11027	1424,08077	0,09197
1425,08308	0,11907	1425,10895	0,04687	1425,10082	0,04439
1426,07866	0,05457	1426,10455	0,01638	1426,09642	0,01983
1427,10085	0,02117				
1428,09855	0,00392				

[Cu$_2$Al](Cp*)$_3$ (2)	
m/z	*I*
558,1454	1
559,1569	0,33351
560,1494	0,91405
561,1427	0,30012
562,1371	0,25417
563,1421	0,0695

5. Crystallography

5.1 Powder X-ray diffraction

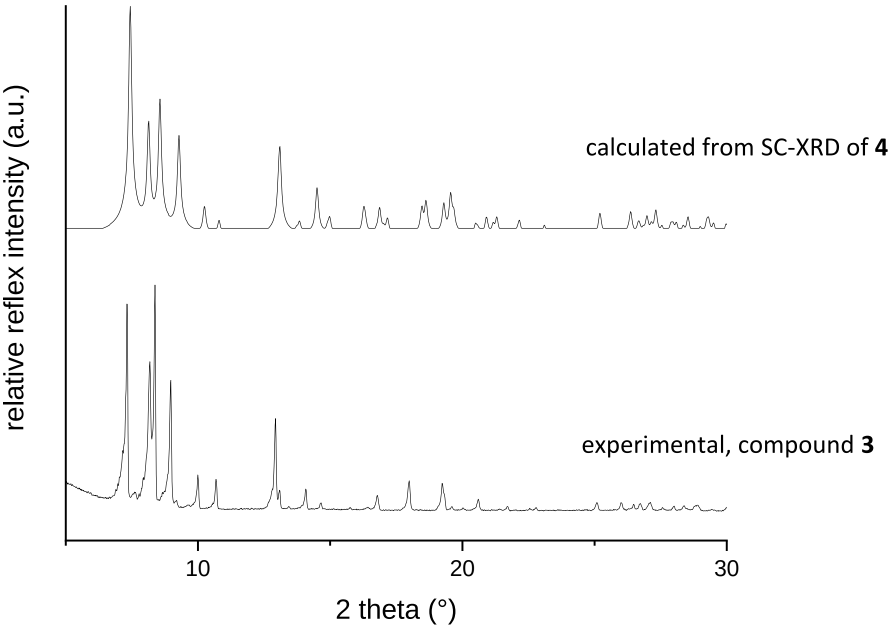

Figure S27: Powder X-ray diffraction pattern of **3/4** (bottom) and calculated pattern based on SC-Xray diffraction data of **3_H/4** (top).

*Note: For compound **3/4**, no SC-XRD data is available due to low quality of the crystals obtained. However, the good agreement between the powder X-ray diffraction pattern of **3/4** and the one calculated from the SC-XRD data of **3_H/4** allows for the conclusion that the two compounds are isostructural.*

5.2 Single crystal X-ray diffraction

Table S4: Crystallographic information for compounds **1, 2, 3_H/4 and 4.**

	1	**2**	**3_H/4**	**4**
chemical formula	$C_{59}H_{86}Cu_4Al_4$	$C_{30}H_{45}Cu_2Al$	$Cu_{7.33}Al_6C_{60}H_{90}$	$Cu_8Al_6C_{60}H_{90}$
formula weight	1157.40	559.74	1438.63	1481.60
temperature	100(2) K	100(2) K	100(2)	100(2)
λ [Å]	0.71073	0.71073	0.71073	0.71073
crystal size [mm]	0.208x0.261x0.815	0.025x 0.055 x 0.075	0.048x 0.102x 0.193	0.093x0.142x0.187
crystal habit	black-green fragment	yellow-orange fragment	black needle	black fragment
crystal system	monoclinic	triclinic	monoclinic	monoclinic
space group	P 21/n	P-1	*I 2/m*	*C 2/m*
unit cell dimensions	a = 14.6563(11) Å b = 25.306(2) Å c= 19.6043(16) Å α = 90° β = 92.589(3)° γ = 90°	a = 10.6817(8) Å b = 10.6837(8) Å c= 15.0961(12) Å α = 75.703(2)° β = 72.180(2)° γ = 60.202(2)°	a = 12.9999(9) Å b = 17.2545(13) Å c = 16.5285(17) Å α = 90° β = 97.7410(16)° γ = 90°	a = 19.603(4)Å b = 17.296(4)Å c = 12.944(2)Å α = 90° β = 123.107(7) γ = 90°
volume [Å^3]	7263.7(10)	1413.85(19)	3673.7(5)	3676.4(13)
Z	4	2	2	2
ρ (calculated) [g/cm^3]	1.058	1.315	1.301	0.158
absorption coefficient [mm^{-1}]	1.232	1.551	2.181	0.583
F(000)	2432	592	1481	163
diffractometer	Bruker D8 Venture Duo IMS	Bruker D8 Venture	Bruker D8 Venture	Bruker D8 Venture Duo IMS
radiation source	IMS microsource, Mo	TXS rotating anode, Mo	TXS rotating anode, Mo	IMS microsource, Mo
θ range for data collection [°]	2.08 – 25.39	2.39-25.76	2.36-25.68	2.355-25.693
index ranges	$-17 \leq h \leq 17$ $-30 \leq k \leq 30$ $-23 \leq l \leq 23$	$-12 \leq h \leq 13$ $-12 \leq k \leq 12$ $-18 \leq l \leq 18$	$-15 \leq h \leq 15$ $-21 \leq k \leq 20$ $-20 \leq l \leq 20$	$-23 \leq h \leq 23$ $-21 \leq k \leq 21$ $-15 \leq l \leq 15$
reflections collected	278735	60165	46509	86379
independent reflections	13338 [(R_{int}) = 0.1132]	5328 [(R_{int}) = 0.0299]	3607 [(R_{int}) = 0.0412]	3610 [(R_{int}) = 0.0271]
coverage of independent reflections	99.9 %	98.6 %	99.9 %	99.9%
absorption correction	Multi-scan	Multi-scan	Multi-scan	Multi-Scan
max. and min. transmission	0.5707 and 0.7452	0.7073 and 0.7452	0.9030 and 0.6780	0.7453 and 0.6940
structure solution technique	direct methods	direct methods	direct methods	direct methods
structure solution program	SHELXS-97 (Sheldrick 2008)	SHELXS-97 (Sheldrick 2008)	SHELXS-13/1 (Sheldrick 2008)	SHELXS-13/1 (Sheldrick 2008)
refinement method	full matrix least squares on F^2	full matrix least squares on F^2	full matrix least squares on F^2	full matrix least squares on F^2

5. Crystallography

refinement program	SHELXL 2014 (Sheldrick 2014)	SHELXL 2014 (Sheldrick 2014)	SHELXL 2014 (Sheldrick 2014)	SHELXL 2018/3 (Sheldrick 2018)
function minimized	$\sum w(F_0^2 - F_c^2)^2$	$\sum w(F_0^2 - F_c^2)^2$	$\sum w(F_0^2 - F_c^2)^2$	$\sum w(F_0^2 - F_c^2)^2$
data/restraints/parameters	13338/840/833	5328/145/334	3607/160/249	3610/217/248
goodness of fit on F^2	1.059	1.269	1.118	1.097
$\Delta/\sigma_{max.}$	0.543	0.001	0.001	0.018
final R indices [I>2σ]	R1 = 0.0718, wR2 = 0.1499	R1 = 0.0389, wR2 = 0.0872	R1 = 0.0572, wR2 = 0.1882	R1 = 0.0790, wR2 = 0.2315
final R indices [all data]	R1 = 0.0960, wR2 = 0.1437	R1 = 0.0405, wR2 = 0.0878	R1 = 0.0683, wR2 = 0.1974	R1 = 0.0816, wR2 = 0.2361
$\Delta F_{max.}$, $\Delta F_{min.}$ [e / Å^{-3}]	0.853, -0.847	0.532, -0.639	0.617, -0.579	2.932/-0.823

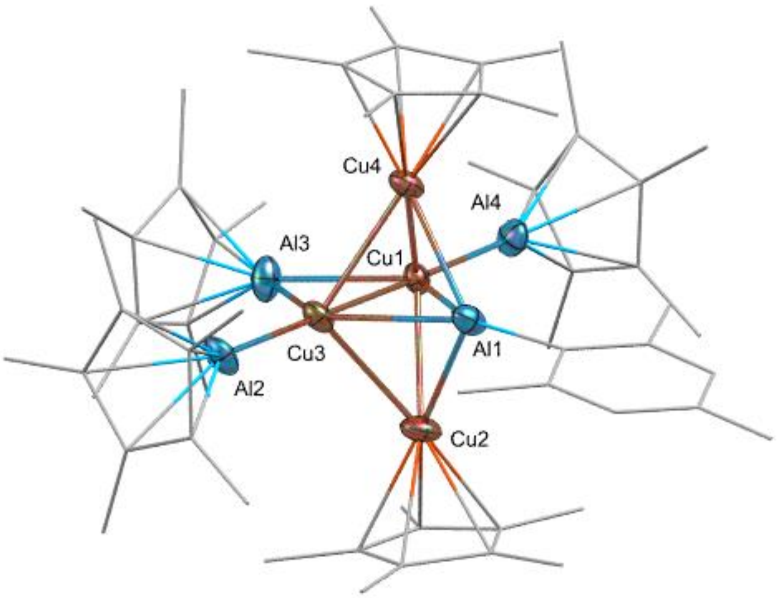

Figure S28: Molecular structure of **1** in the solid state as determined by SC-XRD. Thermal ellipsoids are shown at the 50 % probability level, hydrogen atoms, co-crystallized solvent molecules and disordered groups are omitted for clarity and ligands are simplified as wireframes. Selected interatomic bond distances [Å] and angles [°]: Cu2-Cu3: 2.5335(13), Cu1-Cu2: 2.5441(2), Cu3-Al2: 2.3103(14), Cu1-Al4: 2.3190(14), Cu4-Al1: 2.3519(15) Å; Cu1-Al1: 2.4386(14) Å; Cu1-Al3: 2.4277(16) Å; Cu3-Al3: 2.4261(16) Å; Al3-Cp*$_{centroid}$: 1.906, Al4-Cp*$_{centroid}$: 1.958, Al2-Cp*$_{centroid}$: 1.958, Cu4-Cp*$_{centroid}$: 1.922, Cu2- Cp*$_{centroid}$: 1.900, Al1-C$_{mesitylene}$: 1.966(5), Cu1-Cu2-Cu4: 106.16(4), Cu2-Cu3-Cu4: 107.20(4), Al2-Cu3-Cu1: 179.25(8), Al4-Cu1-Cu3: 178.89(7); Cu1-Al1-Cu3: 57.75(3).

***1** crystallizes in the monoclinic space group P21/n with four molecules per unit cell as well as three heavily disordered toluene molecules per asymmetric unit. **1** consists of a Cu_4(Cu1-Cu4)Al(Al1) trigonal bipyramid, whereby the central Cu_2 unit is additionally coordinated by two "terminal" (Al2, Al4) as well as one bridging (Al3) AlCp* ligand. Interestingly, to the best of our knowledge, **1** is the first crystallographically characterized compound featuring an Al^{I}Mes ligand. The bonding Cu-Cu distances in **1** (mean value 2.541 Å) are within the expected range* _for this class of compounds[5,6]. The Cu-Cu-Cu bond angles are 106.16(4)° (Cu4-Cu1-Cu2) and 107.20(4)° (Cu2-Cu3-Cu4), whereas the central triangle of the bipyramid exhibits a Cu1-Al1-Cu3 angle of 57.75(3)°. The Cu-Al1 and Cu-Al3 distances (2.3519(15) Å (Cu4-Al1); 2.4386(14) Å (Cu1-Al1); 2.4277(16) Å (Cu1-Al3); 2.4261(16) Å (Cu3-Al3)) are slightly longer than the ones of terminally bound AlCp* (2.3103(14) Å (Cu3-Al2); 2.3190(14) Å (Cu1-Al4)). In general, the Cu-Al distances are shorter than those found in $[H_3Cu_6Al_6](Cp^*)_6(PhCHN)$ (2.4027(14) – 2.7189(14) Å)[5] or the Hume Rothery phases $CuAl_2$ (2.587(4))[7] and Cu_9Al_4 (2.468(2) – 2.737(3) Å)[8]. The horizontal axis of **1** is close to linearity with bond angles of 179.25(8)° (Al2-Cu3-Cu1) and 178.89(7)° (Al4-Cu1-Cu3). The Al-Cp$^*_{centroid}$ distances are well comparable to other compounds featuring coordinated AlCp* groups.[9, 10] The Cu-Cp$^*_{centroid}$ distances in **1** are found to be 1.900 Å and 1.922 Å. The Al1-C_{Mes} bond length (1.966(5) Å) is slightly shorter than the Al-C_{Mes} bond found in the corresponding Al(III) compound $AlMes_3$ (1.995(8) Å).[11] It is noted that from an alternate point of view, a Cu_4 butterfly structural motif can be distinguished in the structure of **1**, which is known from other molecular Cu cluster compounds like $[Cu_4Te_4](PiPr)_4$[12] and $[Cu_4](PPh_3)_2(mt)_4$[13] (mt = 2-mercaptothiazoline). Interestingly, similar structural motifs can also be identified in larger Cu/Al clusters. Thus, an Al atom surrounded by four butterfly-like arranged Cu atoms is found in the molecular structure of $[H_4Cu_6Al_6](Cp^*)_6$[5], while in the large cluster $[Cu_{43}Al_{12}](Cp^*)_{12}$, AlCp* occupies positions capping Cu_3 triangular faces.[9] In view of these structural analogies, **1** can be seen as a native "building block" for larger Cu/Al aggregates._

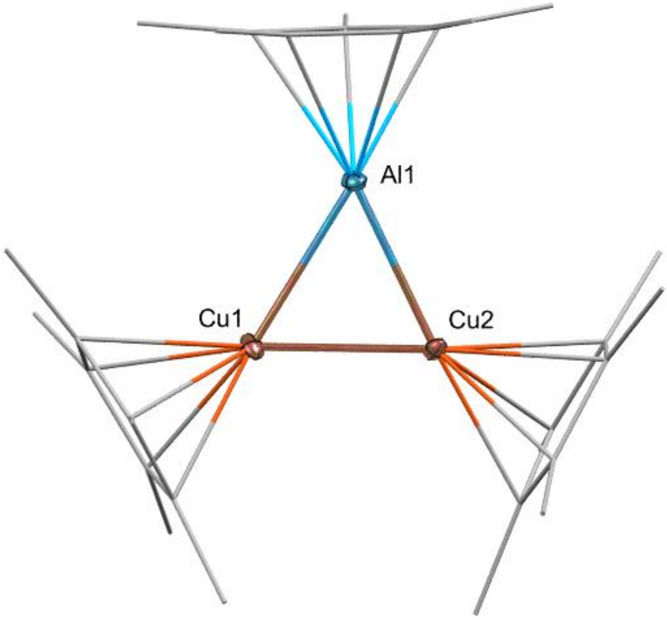

Figure S29: Molecular structure of **2** in the solid state as determined by SC-XRD. Thermal ellipsoids are shown at the 50 % probability level, hydrogen atoms, co-crystallized solvent molecules and the disorder of the metal triangle are omitted for clarity and ligands are simplified as wireframes. Selected interatomic bond distances [Å] and angles [°]: Cu1-Cu2: 2.265(8), Cu2-Al: 2.314(15), Cu1-Al: 2.40(2), Cu1-Cp*$_{centroid}$: 1.942, Cu2-Cp*centroid: 1.920 Å, Al-Cp*$_{centroid}$: 1.933.

*Compound **2** crystallizes in the triclinic space group P-1 with two molecules per unit cell and is isostructural to the related isoelectronic triangular cluster $[CuZn_2](Cp^*)_3$ (see figure 1).[14] The metal distribution within the cluster core is disordered over all three positions. Thus, all structural and geometric parameters involving the metal core are subject to some uncertainty and will therefore be discussed only on a qualitative level. The three metal atoms span an almost equilateral triangle. The Cu1-Cu2 distance (2.265(8) Å) is significantly shorter than in other cluster compounds exhibiting Cu-Cu bonds, such as **1** (mean Cu-Cu bond distance 2.541 Å) or $[H_3Cu_6Al_6](Cp^*)_6(PhNHC)$ (mean distance 2.531 Å)[5]. Also the Cu-Cu distances within the $Cu_3Cp^*_3$ triangle in the trigonal bipyramidal cluster $[Cu_3Zn_4](Cp^*)_5$, (2.442(2)–2.446(2) Å)[15] are distinctly longer than in **2**. The two Cu-Al distances in **2** (2.314(15) Å and 2.40(2)) are comparable to those found in $[H_3Cu_6Al_6](Cp^*)_6(PhNHC)$ [5] or Hume Rothery Cu/Al solid state structures (vide supra)[7, 8]. The Cu-$Cp^*_{centroid}$ distances in **2** (1.942 Å and 1.920 Å) are slightly longer than those in related compounds [14, 15] , whereas the Al-$Cp^*_{centroid}$ distance (1.933 Å) is within the range for complexes and clusters of AlCp* with transition metals.[5, 10]*

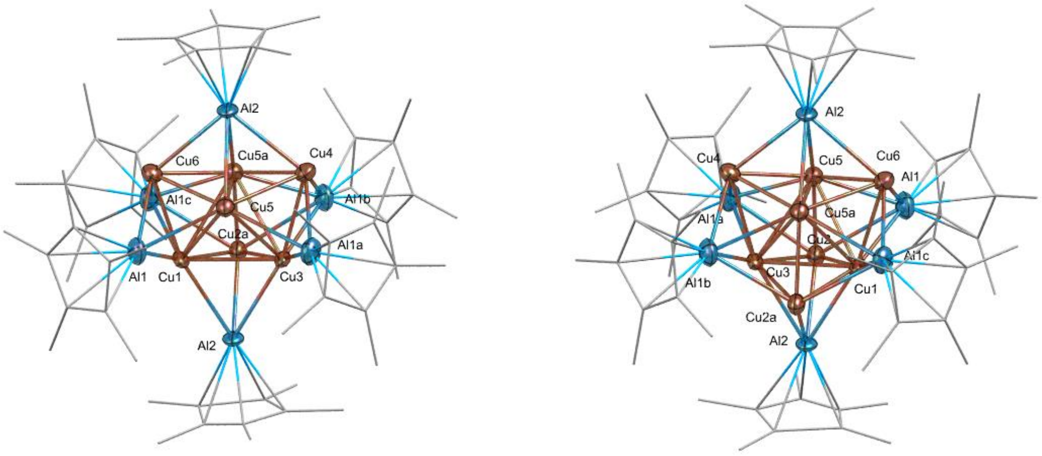

Figure S30: Molecular structure of **3_H/4** in the solid state as determined by SC-XRD, the two co-crystallizing cluster **3_H** (left) and **4** (right) are shown separately. Thermal ellipsoids are shown at the 50 % probability level, hydrogen atoms, co-crystallized solvent molecules and disordered groups are omitted for clarity and ligands are simplified as wireframes. Selected interatomic bond distances [Å] and angles [°]: Cu1-Cu2: 2.311(3), Cu1-Cu5: 2.626(2), Cu1-Cu6: 2.381(2), Cu1-Cu3: 2.563(2), Cu2-Cu3: 2.314(3), Cu3-Cu5: 2.625(2), Cu3-Cu4: 2.390(2), Cu2-Cu5: 2.326(3), Cu6-Cu5: 2.404(2), Cu4-Cu5: 2.396(2), Cu1-Al1: 2.4850(15), Cu2-Al1: 2.588(2), Cu5-Al1: 2.4966(18), Cu6-Al1: 2.5193(16), Cu1-Al2: 2.450(2), Cu2-Al2: 2.528(2), Cu3-Al2: 2.477(2), Al2-$Cp^*_{centroid}$: 1.94, Al1-$Cp^*_{centroid}$: 1.96; Cu5-Cu5a-Cu3: 59.0, Cu3-Cu1-Cu5: 60.77(5), Cu2-Cu1-Cu2a: 108.83(12), Cu1-Cu2-Cu3: 67.31(9), Cu2-Cu4-Cu2a: 58.9, Al1-Al1a-Al1b-A1c: 0.0, Al2-Al1b-Al2a-Al1: 0.0.

*Compounds **3_H/4** co-crystallize in the monoclinic space group I2/m with two molecules per unit cell. In general, the structure compromises a core of two nested copper tetrahedra embedded into an AlCp* octahedron. Hereby, the outermost Cu positions (Cu2) are only partially occupied,* *being well consistent with a composite of [HCu_7Al_6](Cp*)$_6$ and [Cu_8Al_6](Cp*)$_6$ as determined by LIFDI-MS (vide supra). The hydride could not be located by SC-XRD but DFT calculations allow for an assessment of its binding mode (vide infra). The faces of the inner Cu tetrahedron (Cu1, Cu3, Cu5) are capped by the Cu atoms (Cu2, Cu2a, Cu4, Cu6) of the outer Cu tetrahedron resulting in an overall structural motif, which is well known from corresponding Hume-Rothery phases like γ-brass (Cu_5Zn_8) or Cu_9Al_4. Additionally, the tetracapped tetrahedron to tricapped tetrahedron relationship is documented in the literature for copper clusters, although for Cu(I).[16, 17] The structure can be also be described as a superposition of two AlCp* capped Cu-butterfly motifs (Cu4, Cu5, Cu5a, Cu6 / Cu1, Cu2, Cu2a, Cu3) giving a structural analogy to compound* ***1****. Cu-Cu distances vary between 2.311(3) Å (Cu1-Cu2) and 2.703 Å (Cu5-Cu5a) with a mean value of 2.447 Å, which is slightly shorter than in* ***1*** *or the closely related molecules [$H_3Cu_6Al_6$](Cp*)$_6$(PhCHN) and [$Cu_{43}Al_{12}$](Cp*)$_{12}$. The Cu-Cu distances inside the inner Cu tetrahedron are thereby longer than those connecting the inner tetrahedron with the capping Cu atoms. The triangular faces of the inner tetrahedron span almost equilateral triangles with bond angles close to 60 ° (e.g. Cu5-Cu5a-Cu3: 59.0 °; Cu3-Cu1-Cu5: 60.77(5) °). The acute and obtuse angles between the outer and inner Cu tetrahedron vary between 108.83(12) ° (Cu2-Cu1-Cu2a) and 67.31(9) ° (Cu1-Cu2-Cu3). The outer tetrahedron itself is spanned by almost equilateral triangles (e.g. Cu2-Cu4-Cu2a: 58.9 °; Cu4-Cu6-Cu2a: 59.7 °). Al-Cu distances vary between 2.450(2) Å (Al2-Cu1) and 2.588(3) Å (Al1-Cu2). The mean Cu-Al distance of 2.51 Å is slightly longer than in* ***1*** *and* ***2****, but very similar to the mean distance in the solid-state phase $CuAl_2$ (vide supra). Very interestingly, the AlCp* shell adopts a perfect octahedral shape with dihedral angles of 0.0° between Al1-Al1a-Al1b-Al1c and Al2a-Al1-Al2-Al1b. Al-Cp*$_{centroid}$ distances are with 1.94 Å (Al2-Cp*$_{centr.}$) and 1.96 Å (Al1-Cp*$_{centr.}$) very similar to those in* ***1****,* ***2*** *as well as [$Cu_{43}Al_{12}$](Cp*)$_{12}$ (vide supra).*

6. Additional experimental data (ATR-IR, TEM, GC-MS)

6.1 ATR-IR data

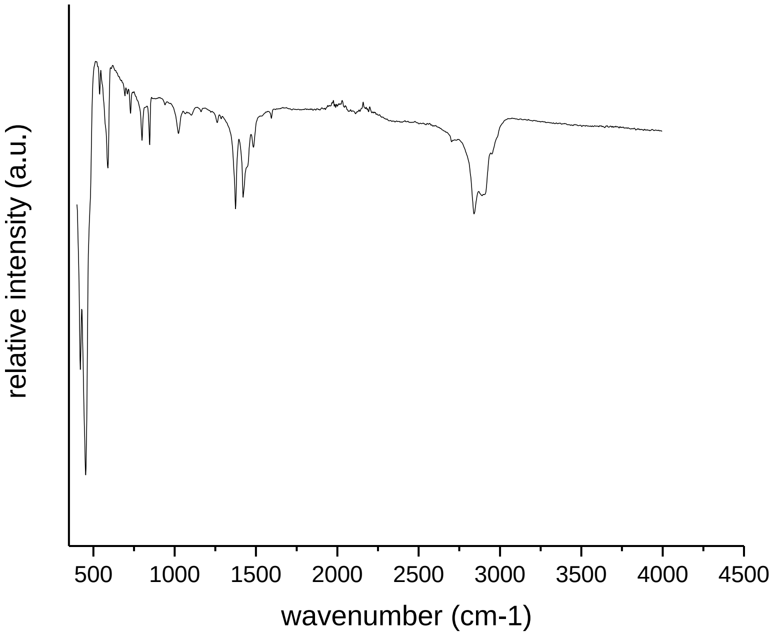

Figure S31: ATR-IR spectrum of $[Cu_4Al_4](Cp^*)_5(Mes)$ (**1**).

6. Additional experimental data (ATR-IR, TEM, GC-MS)

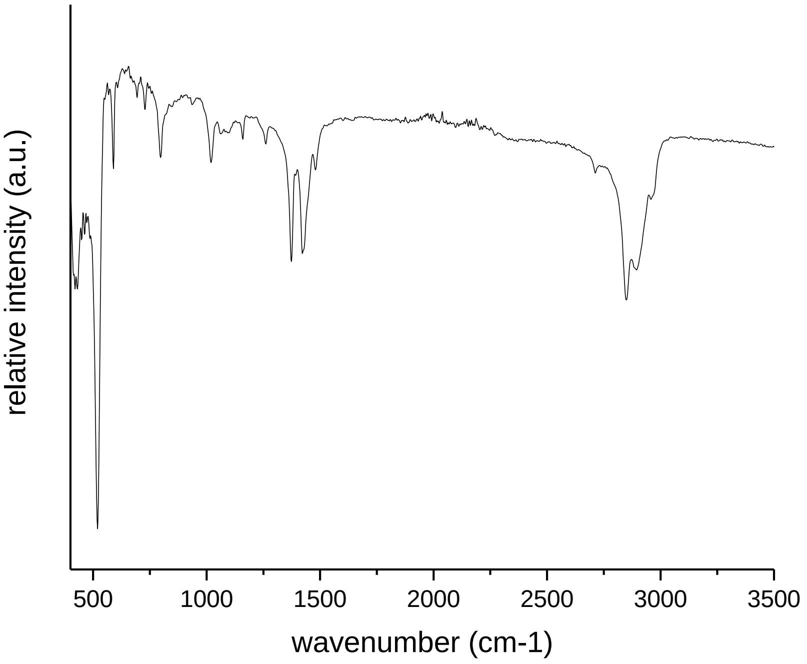

Figure S32: ATR-IR spectrum of **2**.

*The ATR-IR spectrum of **2** is very similar to that of **1**, a very strong signal at 519.1 cm^{-1} is tentatively attributed to metal-metal vibrations of the M_3 triangle. Results from elemental analysis are consistent with calculated elemental composition.*

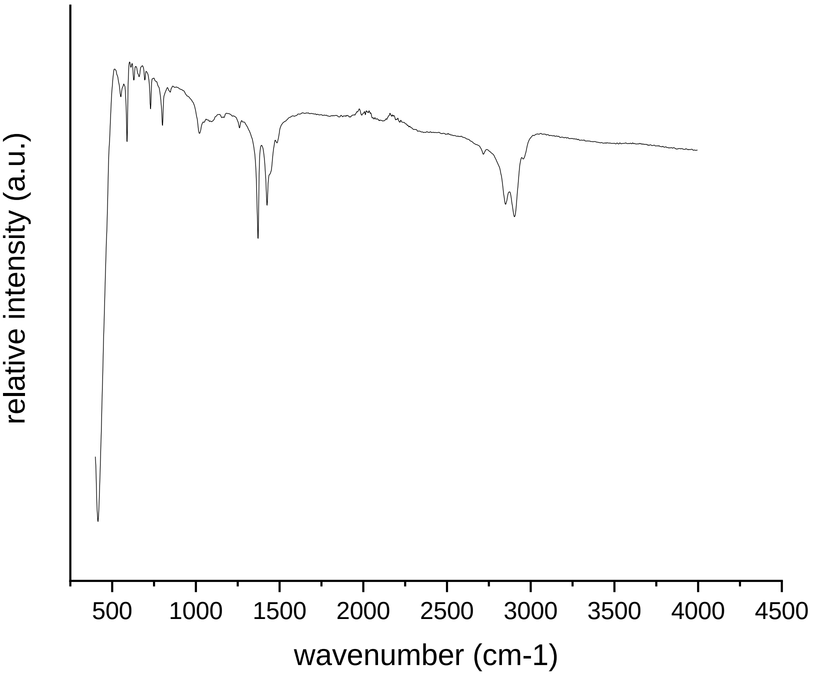

Figure S33: ATR-IR spectrum of compound **3/4**.

6.2 TEM data

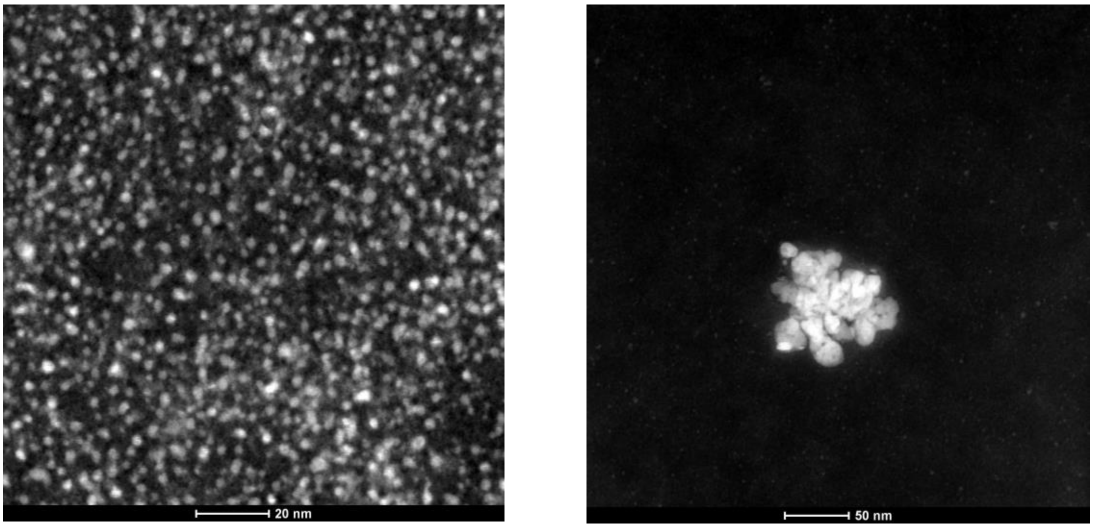

Figure S34: Left: TEM image of evaporated reaction solution of CuMes + **2** (conditions E in Table S1); Right: TEM image of evaporated reaction solution of CuMes +**3/4** (conditions D in Table S1).

6.3 GC-MS results

Table S5: Reaction conditions applied in C-H and Si-H activation reactions with isolated **3/4** and reaction products observed by LIFDI-MS (cluster species) and GC-MS (organic species).

silane species added	solvent	product cluster observed in LIFDI-MS	species identified by GC-MS
$(TMS)_3SiH$	**toluene-h_8**	**3/3_H/4; {$[Cu_7Al_6](Cp^*)_6(Si(TMS)_3)$ – H}, {$[Cu_8Al_6](Cp^*)_6(Si(TMS)_3)$ – H}**	**$HSiMe_3$:** m/z = 73.1 $[-H]^+$, 59.1 $[-Me]^+$ **HMe_2Si-$SiMe_3$**:[19] m/z = 133 $[+H]^+$, 117 $[-Me]^+$, 103 $[-2xMe]^+$, 87 $[-3xMe]^+$, 73 $[-HMe2Si]^+$, 59 $[-HMe2Si, -Me]^+$ **Me_3Si-$SiMe_3$**:[20] m/z = 147.1 $[+H]^+$, 131 $[-Me]^+$, 117 $[-2xMe]^+$, 103 $[-3xMe]^+$, 87 $[-4xMe +H]^+$, 73 $[-SiMe3]^+$, 59 $[-Me, -SiMe3]^+$ **Me_3Si-SiH_2-$SiMe_3$**:[21] 176.1 $[M]^+$, 161.0 $[-Me]^+$, 145.0 $[-2xMe, -H]^+$, 131 131 $[-3xMe]^+$, 117 $[-4xMe +H]^+$,101 $[-SiMe3, -2H]^+$, 88 $[SiMe_4]^+$, 73 $[SiMe_3]^+$, 59 $[SiMe_2]^+$ **$(C_7H_7)Si((TMS)_3$:**[22] m/z = 341.1 $[+ 3H]^+$, 325 $[-Me + 2H]^+$, 267 $[-SiMe_3 + H]$, 253 $[-SiMe3, -Me, +3H]^+$, 236 $[-SiMe3, -2xMe, +H]^+$, 193 $[-2xSiMe3, +H]^+$, 154, 133 $[HMe_2Si\text{-}SiMe_3 +H]^+$, 87, 73 $[SiMe_3]^+$, 59 $[HSiMe_2]^+$;
$(TMS)_3SiH$	**toluene-d_8**	**3/3_H/4; {$[Cu_7Al_6](Cp^*)_6(Si(TMS)_3)$ – H}, {$[Cu_8Al_6](Cp^*)_6(Si(TMS)_3)$ – H}**	**$HSiMe_3$:** m/z = 73.1 $[-H]^+$, 59.1 $[-Me]^+$ **$(HSiMe_2)_2(SiMe_3)SiH$:** m/z = 220.2 $[M]^+$, 205.2 $[-Me]^+$, 177, 161, 145.1, 129.1, 105.1, 91.0, 73.0, 57.1
$(TMS)_3SiD$	**toluene-h_8**	**3/3_H/3_D/4**	
$(TMS)_4Si$	**toluene-d_8**	**3/3H/4; {$[Cu_8Al_6](Cp^*)_6(SiMe_3)$ – H}**	**Pentamethylfulvene:**[*] m/z = 134.1 $[M]^+$, 119.1 $[-Me]^+$, 103 $[- 2x Me -H]^+$, 103, 91, 77, 51; **$(TMS)_3SiH$:**[*] 248.1, 207, 190.9, 174.1 $[-SiMe_3H]^+$, 159.0, 145.0, 129.0, 91.0, 73.1, 59.0;
none	**toluene-h_8**	**3/3_H/4**	**Pentamethylfulvene:**[*] m/z = 134.1 $[M]^+$, 119.1 $[-Me]^+$, 103 $[- 2x Me -H]^+$, 103, 91, 77, 51
none	**toluene-d_8**	**3/4**	
none	**methyl-cyclo-hexane**	**3/4**	

[*]: identified by software database

Note: As expected, HCp was detected in all GC experiments resulting from protolytic cleavage of the cluster species during sample preparation. Additionally, several silyl ether species/silanol species were detected, probably formed by oxidation during sample preparation or due silicon grease impurities.*

*It is noted that no C-H activation was observed with simple alkanes such as methylcyclohexane. The substrate scope of C-H activations realizable by **3** will be subject of further research in our group.*

7. DFT calculations: Supplementary data

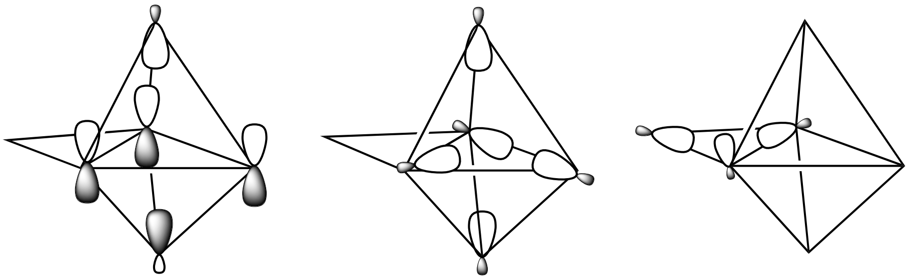

Scheme S5: Sketches of the three bonding MO containing the six electrons associated with the Cu_4Al_2 core of **1**.

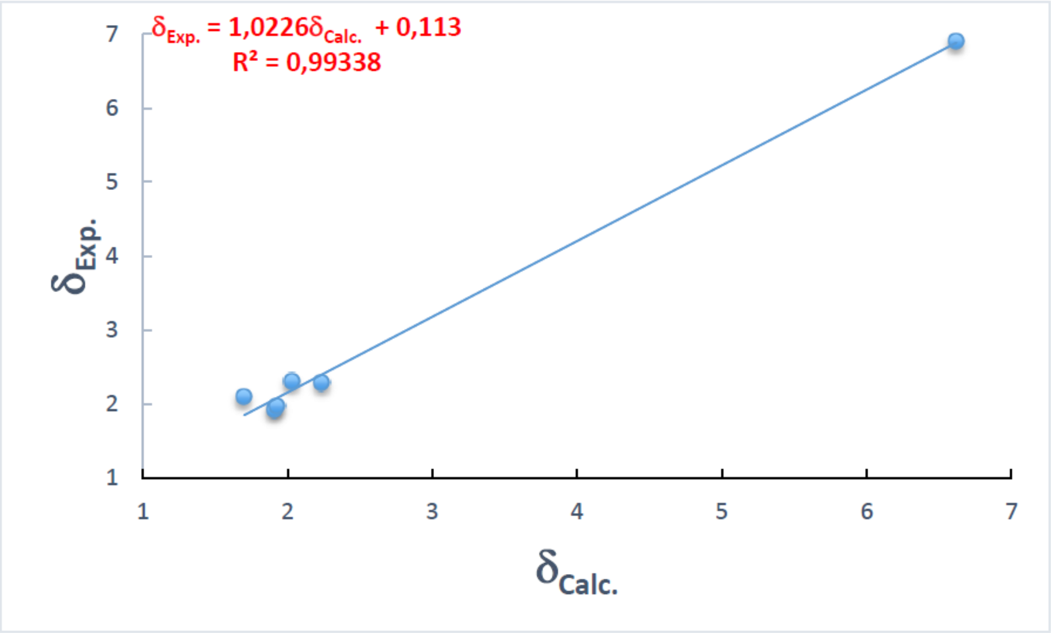

Figure S35: Correlation between experimental (δ_{Exp}) and DFT-computed (δ_{Calc}) ^1H NMR chemical shifts for **1.**

7. DFT calculations: Supplementary data

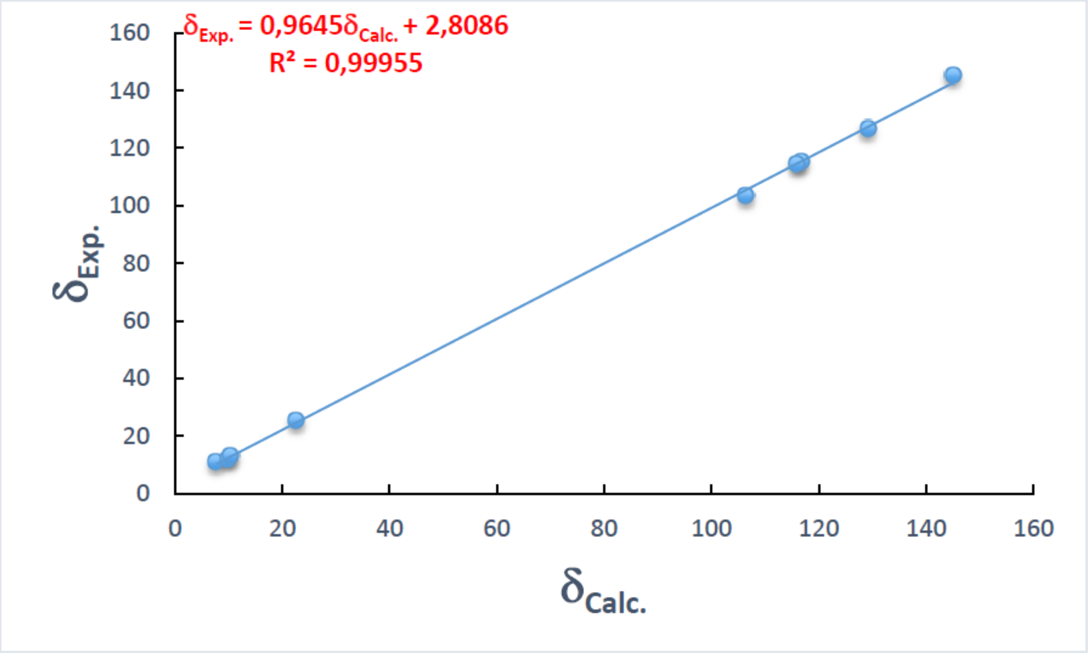

Figure S36: Correlation between experimental (δ_{Exp}) and DFT-computed (δ_{Calc}) ^{13}C NMR chemical shifts for **1**.

Table S6: Relevant computed data for **1.** Distances are in Å. WBI = Wiberg bond index).

HOMO-LUMO Gap (eV)			**1.28**		
NBO charges within the Cu_4Al bipyramid	**Cu1**	**Cu3**	**Cu2**	**Cu4**	**Al1**
	0.15	0.15	0.40	0.41	0.50
NBO charges of μ_2- and terminal Al	**Al3**	**Al2**	**Al4**		
	0.69	0.83	0.86		
Within the Cu_4Al bipyramid	**Dist. [WBI]**		**(μ_2-Al)-Cu**	**Dist. [WBI]**	
Al1-Cu1	2.445 [0.250]		Al3-Cu1	2.398 [0.297]	
Al1-Cu3	2.476 [0.251]		Al3-Cu3	2.435 0.266	
Al1-Cu2	2.363 [0.510]		**Terminal Al-Cu**	**Dist. [WBI]**	
Al1-Cu4	2.390 [0.479]		Al4-Cu1	2.294 [0.442]	
Cu2-Cu1	2.522 [0.071]		Al2-Cu3	2.302 [0.431]	
Cu2-Cu3	2.562 [0.042]				
Cu4-Cu1	2.543 [0.061]				
Cu4-Cu3	2.484 [0.104]				
Cu1-Cu3	2.441 [0.045]				

7. DFT calculations: Supplementary data

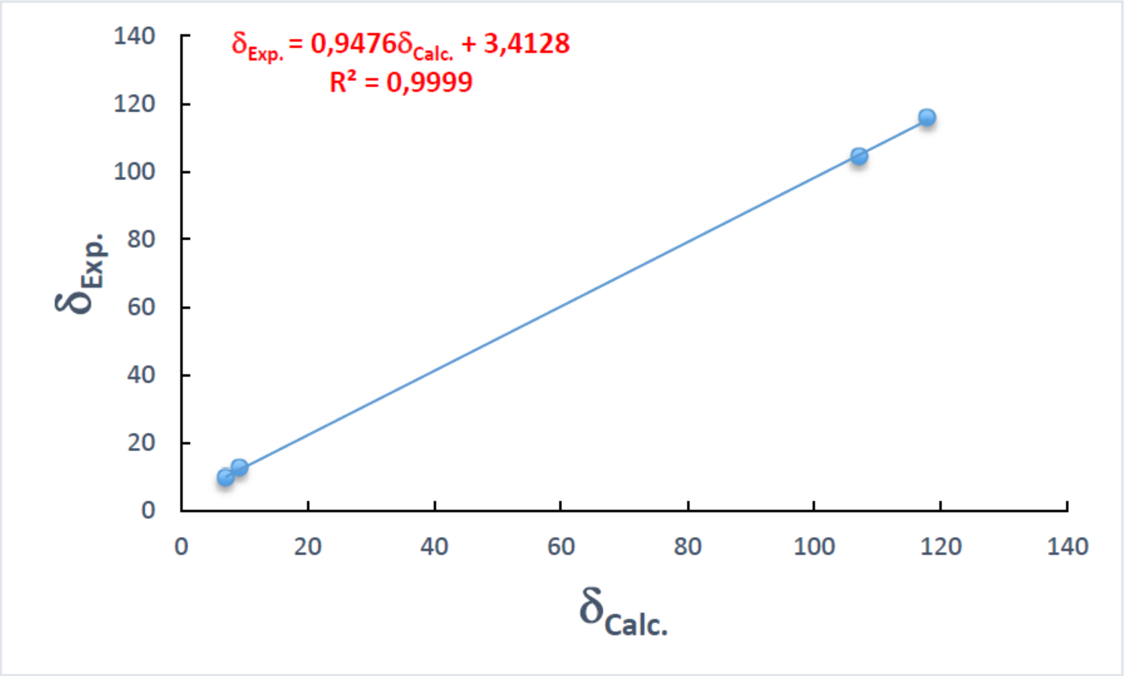

Figure S37: Correlation between experimental (δ_{Exp}) and DFT-computed (δ_{Calc}) ^{13}C NMR chemical shifts for **2**.

7. DFT calculations: Supplementary data

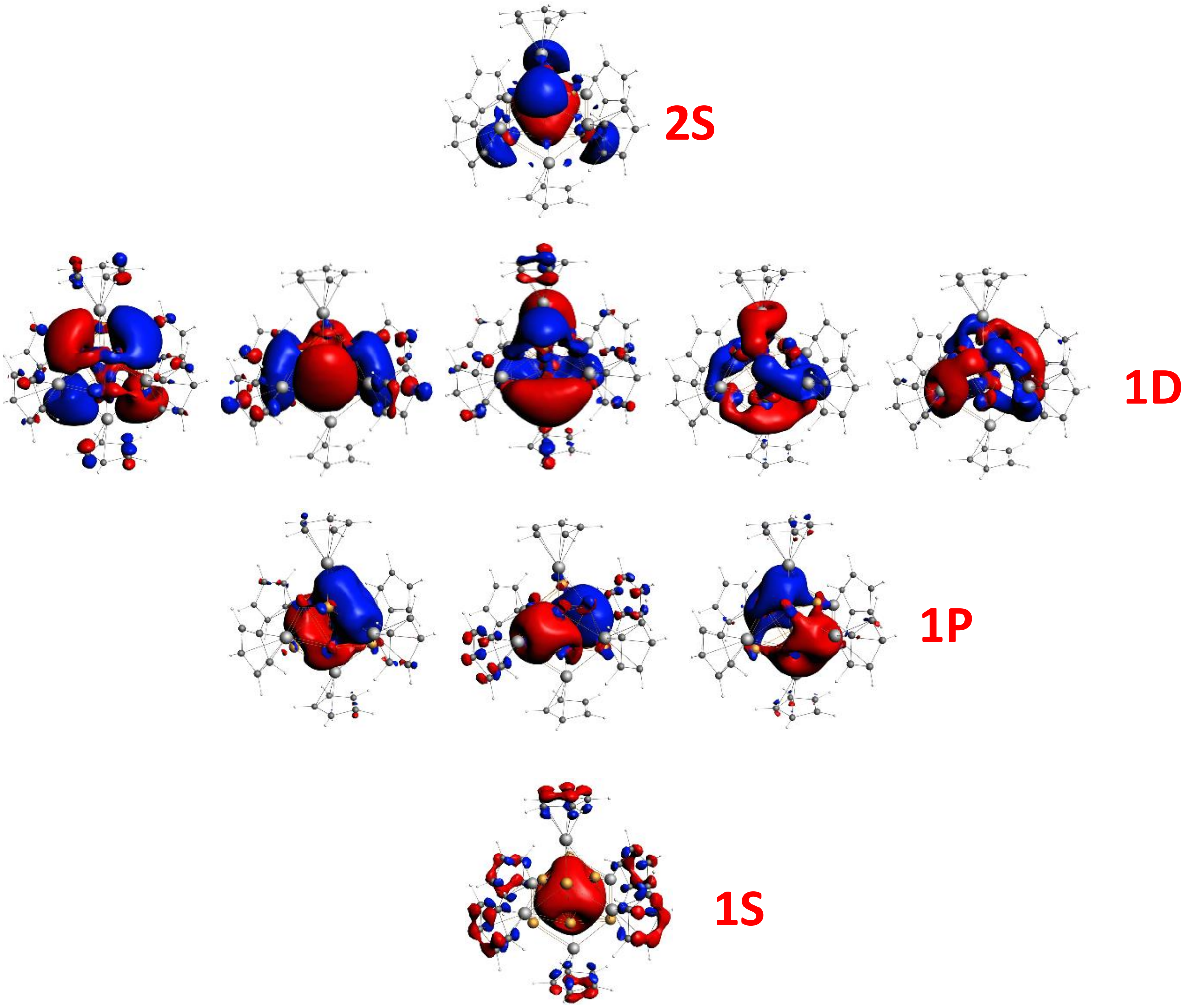

Figure S38: The ten bonding Kohn-Sham orbitals containing the 20 electrons in the simplified superatom model $[Cu_8Al_6](Cp)_6$. They are composed by more than 85% of that of $[Cu_8Al_6]^{6+}$ shown in Figure S41. Similar results are obtained for the real cluster $[Cu_8Al_6](Cp^*)_6$ (**4**), but with more mixing with ligand levels.

7. DFT calculations: Supplementary data

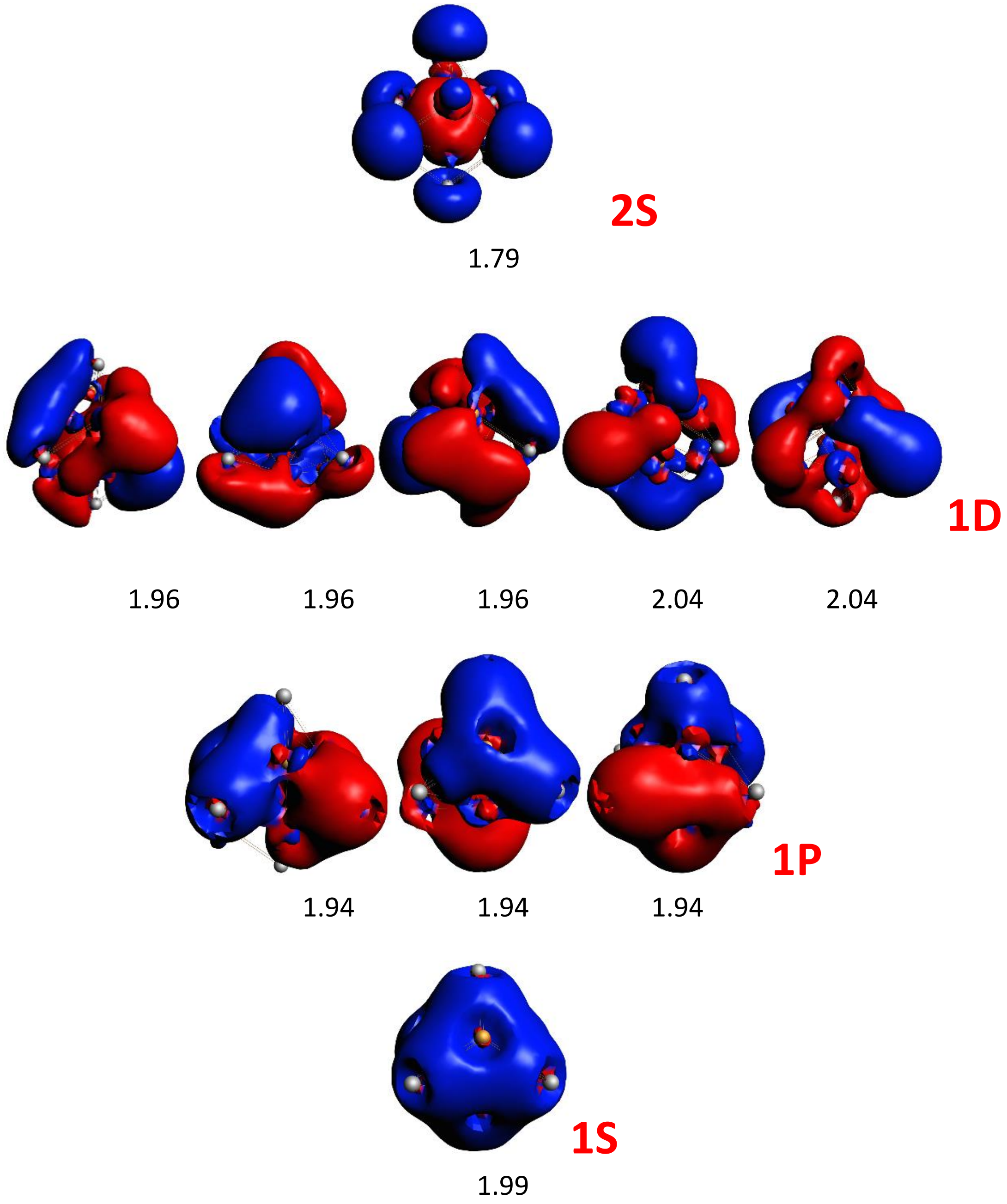

Figure S39: The ten bonding Kohn-Sham orbitals containing the 20 electrons in the simplified superatomic $[Cu_8Al_6]^{6+}$ inner core of the $[Cu_8Al_6](Cp)_6$ model, and which generate the ten jellium orbitals of $[Cu_8Al_6](Cp)_6$. The numerical values indicate the occupation (in electron) of the $[Cu_8Al_6]^{6+}$ orbitals in the $[Cu_8Al_6](Cp)_6$ model, as calculated by the ADF program on the basis of its interaction with the $(Cp_6)^{6-}$ fragment.

Table S7: Relevant computed data for **4**, **3** and **3_H**. Distances are in Å. WBI = Wiberg bond index (in brackets). Values in parenthesis are the numbers of averaged quasi-equivalent atoms, owing to the fact that **4** is pseudo-T_h, whereas **3**, **3_H(a)** and **3_H(a)** are close to 3-fold symmetry.

Compound		**4**	**3**	**3_H(a)**	**3_H(b)**
HOMO-LUMO Gap (eV)		1.17	-	1.16	1.81
NBO charges (av.)	Cu(inner)	0.16 (4)	0.16 (3) 0.34 (1)	0.25 (3) 0.33 (1)	0.28 (3) 0.25 (1)
	Cu(cap)	0.24 (4)	0.21 (3)	0.26 (3)	0.23 (3)
	Al	0.28 (6)	0.21 (3) 0.45 (3)	0.16 (3) 0.49 (3)	0.48 (3) 0.26 (3)
	μ_3-H			-0.35	-0.58
Distances [WBI]	(μ_3-H)-Cu (av. and range)			1.795 [0.128] 1.788-1.800	1.810 [0.045] 1.807-1.813
	Cu(inner)-Cu(inner) (av. and range)	2.745 [0.030]	2.941 [0.026] 2.568-3.318	3.085 [0.022] 2.599-3.616	3.047 [0.014] 2.586-3.457
	Cu(cap)-Cu(inner) (av. and range)	2.505 [0.023]	2.580 [0.023] 2.502-2.684	2.535 [0.030] 2.438-2.598	2.573 [0.021] 2.489-2.753
	Al-Cu(cap) (av. and range)	2.530 [0.289]	2.494 [0.300] 2.413-2.625	2.524 [0.279] 2.396-2.762	2.505 [0.301] 2.405-2.737

8. Supplementary Figure for conclusion and perspectives

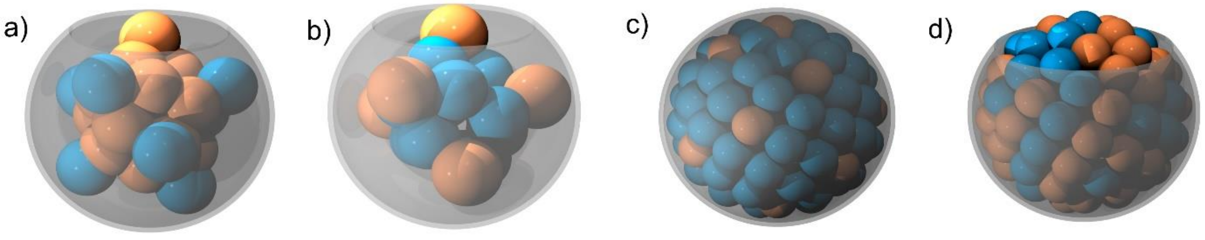

Figure S40: Conceptual models for intermetalloid clusters of TM/E (TM = transition metal, E = group 12/13 metal) combination highlighting our research perspectives. a) Small core-shell cluster with reactive TM site. The $[Cu_7Al_6](Cp^*)_6$ cluster from this work falls in this class. b) Small core-shell cluster with inverted core composition. c) Large, ligand protected core-shell cluster. d) Large intermetalloid cluster with random elemental distribution and open coordination site.

9. References for Materials and Methods

C1) *APEX suite of crystallographic software*, APEX 3, Version 2015-5.2, Bruker AXS Inc., Madison, Wisconsin, USA, 2015.

C2) *SAINT*, Version 8.34A, Bruker AXS Inc., Madison, Wisconsin, USA, 2014.

C3) *SADABS*, Version 2014/5, Bruker AXS Inc., Madison, Wisconsin, USA, 2012.

C4) G. M. Sheldrick, *Acta Crystallogr. Sect. A,* 2015, **71**, 3–8.

C5) G. M. Sheldrick, *Acta Crystallogr. Sect. C,* 2015, **71**, 3–8.

C6) C. B. Hübschle, G. M. Sheldrick, B. Dittrich, *J. Appl. Cryst.* 2011, **44**, 1281–1284

C7) *International Tables for Crystallography, Vol. C* (Ed.: A. J. Wilson), Kluwer Academic Publishers, Dordrecht, The Netherlands, 1992, Tables 6.1.1.4 (pp. 500–502), 4.2.6.8 (pp. 219–222), and 4.2.4.2 (pp. 193–199).

C8) A. L. Spek, *Acta Crystallogr. Sect. C,* 2015, **71**, 9–18.

C9) A. L. Spek, *Acta Crystallogr. Sect. D,* 2009, **65**, 148–155.

C10) C. F. Macrae, I. J. Bruno, J. A. Chisholm, P. R. Edgington, P. McCabe, E. Pidcock, L. Rodriguez-Monge, R. Taylor, J. van de Streek, P. A. Wood, *J. Appl. Cryst.* 2008, 41, 466–470.

C11) Parr, R.G.; Yang, W. *Density-Functional Theory of Atoms and Molecules*., 1994, Oxford University Press, UK.

C12) a) G. te Velde, F.M. Bickelhaupt, S.J.A. van Gisbergen, C.F. Guerra, E.J. Baerends, J.G. Snijders, T. Ziegler, *J. Comput. Chem.* 2001, **22,** 931-967;
b) ADF2016, SCM, Theoretical Chemistry, Vrije Universiteit: Amsterdam, The Netherlands; http://www.scm.com.

C13) S. Grimme, S, *J. Comput. Chem.*, 2006, **27,** 1787–1799.

C14) E.V. Lenthe, E.J. Baerends, *J. Comput. Chem.,* 2003, **24,** 1142–1156.

C15) A.D. Becke, *Phys. Rev. A,* 1988, **38**, 3098–3100.

C16) J.P. Perdew, *Phys. Rev. B*, 1986, **33**, 8822–8824.

C17) E.D. Glendening, J.K. Badenhoop, A.E. Reed, J.E. Carpenter, J.A. Bohmann, C.M. Morales, F. Weinhold, NBO 6.0, Theoretical Chemistry Institute, University of Wisconsin (Madison, WI, **2001**, http://nbo6.chem.wisc.edu).

C18) G. Schreckenbach, T. Ziegler, *J. Phy. Chem*., 1995, **99**, 606-611.

C19) J. G. Snijders and E.J. Baerends, *Mol. Phys.*, 1978, **36**, 1789.

10. References for synthesis and discussion of analytical data

1. E. M. Meyer, S. Gambarotta, C. Floriani, A. Chiesi-Villa and C. Guastini, *Organometallics*, 1989, **8**, 1067-1079.
2. C. Ganesamoorthy, S. Loerke, C. Gemel, P. Jerabek, M. Winter, G. Frenking and R. A. Fischer, *Chem. Comm.*, 2013, **49**, 2858-2860.
3. M. S. Eberhart, J. R. Norton, A. Zuzek, W. Sattler and S. Ruccolo, *J. Am. Chem. Soc.*, 2013, **135**, 17262-17265.
4. H.-J. Himmel and J. Vollet, *Organometallics*, 2002, **21**, 5972-5977.
5. C. Ganesamoorthy, J. Weßing, C. Kroll, R. W. Seidel, C. Gemel and R. A. Fischer, *Angew. Chem. Int. Ed.*, 2014, **53**, 7943-7947.
6. W, G., Wyckoff," *Crystal Structures*,". Interscience Publishers, NY: 1963
7. Y. Grin, F. R. Wagner, M. Armbrüster, M. Kohout, A. Leithe-Jasper, U. Schwarz, U. Wedig and H. G. von Schnering, *J. Solid State Chem.*, 2006, **179**, 1707-1719.
8. L. Arnberg and S. Westman, *Acta Crystallogr. A.*, 1978, **34**, 399-404.
9. J. Weßing, C. Ganesamoorthy, S. Kahlal, R. Marchal, C. Gemel, O. Cador, A. C. Da Silva, J. L. Da Silva, J. Y. Saillard and R. A. Fischer, *Angew. Chem. Int. Ed.*, 2018, **57**, 14630-14634.
10. B. Buchin, T. Steinke, C. Gemel, T. Cadenbach and R. A. Fischer, *Z. anorg. allg. Chem.*, 2005, **631**, 2756-2762.
11. J. J. Jerius, J. M. Hahn, A. M. Rahman, O. Mols, W. H. Ilsley and J. P. Oliver, *Organometallics*, 1986, **5**, 1812-1814.
12. D. Fenske and J. C. Steck, *Angew. Chem. Int. Ed.*, 1993, **32**, 238-242.
13. J. P. Fackler, C. A. López, R. J. Staples, S. Wang, R. Winpenny and R. P. Lattimer, *J. Chem. Soc., Chem. Commun.*, 1992, 146-148.
14. K. Freitag, C. Gemel, P. Jerabek, I. M. Oppel, R. W. Seidel, G. Frenking, H. Banh, K. Dilchert and R. A. Fischer, *Angew. Chem. Int. Ed.*, 2015, **54**, 4370-4374.
15. H. Banh, J. Hornung, T. Kratz, C. Gemel, A. Pöthig, F. Gam, S. Kahlal, J.-Y. Saillard and R. A. Fischer, *Chem. Sci.*, 2018, **9**, 8906-8913.
16. C. Latouche, S. Kahlal, Y.-R. Lin, J.-H. Liao, E. Furet, C. Liu and J.-Y. Saillard, *Inorg. Chem.*, 2013, **52**, 13253-13262.
17. P.-K. Liao, C.-S. Fang, A. J. Edwards, S. Kahlal, J.-Y. Saillard and C. Liu, *Inorg. Chem.*, 2012, **51**, 6577-6591.
18. U. Herzog and G. Roewer, *J. Organomet. Chem.*, 1997, **527**, 117-124.
19. L. Gusel'nikov, Y. P. Polyakov, E. Volnina and N. Nametkin, *J. Organomet. Chem.*, 1985, **292**, 189-203.
20. S. Kashimura, M. Ishifune, N. Yamashita, H.-B. Bu, M. Takebayashi, S. Kitajima, D. Yoshiwara, Y. Kataoka, R. Nishida and S.-i. Kawasaki, *J. Org. Chem.,* 1999, **64**, 6615-6621.
21. M. Mohamed and M. A. Brook, *Can. J. Chem.*, 2000, **78**, 1357-1362.
22. M. J. Sanganee, P. G. Steel and D. K. Whelligan, *J. Org. Chem.*, 2003, **68**, 3337-3339.